Coral Reefs
https://doi.org/10.1007/s00338-024-02500-0

REPORT

A new type of *Halimeda* bioherm on the Queensland Plateau, NE Australia

Jesus Reolid[1] · Or M. Bialik[2,3] · Sebastian Lindhorst[4] · Jan Oliver Eisermann[4] · Alexander Petrovic[5,6] · Carola Hincke[4] · Robin J. Beaman[7] · Jody M. Webster[8] · Christian Betzler[4]

Received: 31 December 2023 / Accepted: 28 April 2024

Abstract Morphology, internal structure, and in situ facies distribution of mesophotic *Halimeda* bioherms from the Queensland Plateau (NE Australia) are presented based on hydroacoustic and oceanographic data, seafloor observations, and discrete sediment sampling carried out during RV SONNE cruise SO292 in 2022. *Halimeda* buildups consist of cone-like mounds up to 500 m in diameter and 3–10 m high, with gentle slopes (2°–5° on the top of Tregrosse Bank). Bioherms occur in water depths of 10–70 m, with most bioherm between 50 and 65 m. Their internal structure consists of aggrading low-amplitude reflections at the core of the bioherm interfingering with high-amplitude reflections to the flanks. Surface facies distribution displays one to four facies belts, from distal to proximal: *Halimeda* rudstone, *Halimeda* rudstone with living plants, *Halimeda* rudstone with coralgal debris, and coralgal boundstone (when present, occupied the top of the bioherms). It is proposed that the alternation of two key processes contributes to the formation of these bioherms: (1) in situ accumulation of *Halimeda* debris and (2) episodic dismantling of the mesophotic coralgal boundstone at the centre of the bioherm by severe storms. These storms may dismantle the mesophotic reef and export coralgal rubble to the flanks. Flanks may be recolonized by *Halimeda* during fair-weather periods. Due to their different geomorphic expressions, complex internal structure, and surficial facies distribution, we suggest that the buildups of the Queensland Plateau represent a new *Halimeda* bioherm morphotype, distinct from previously described bioherms on the adjacent Great Barrier Reef and elsewhere globally.

Keywords Bioherm · Mesophotic reef · Green algae · Carbonate platform · Coral Sea, Australia

✉ Jesus Reolid
jreolid@ugr.es

1 Departamento de Estratigrafía y Paleontología, Universidad de Granada, Avenida Fuentenueva s/n, 18071 Granada, Spain

2 Dr. Moses Strauss Department of Marine Geosciences, Leon H. Charney School of Marine Sciences, University of Haifa, Haifa, Israel

3 Institut für Geologie und Paläontologie, Westfälische Wilhelms-Universität Münster, Münster, Germany

4 Institut für Geologie, Universität Hamburg, Bundesstr. 55, 20146 Hamburg, Germany

5 King Abdullah University of Science and Technology, ANPERC, Thuwal, Saudi Arabia

6 CARMEUSE, Louvain-la-Neuve, Belgium

7 College of Science and Engineering, James Cook University, PO Box 6811, Cairns, QLD 4870, Australia

8 Geocoastal Research Group, School of Geosciences, The University of Sydney, Sydney, Australia

Introduction

Bioherms are in situ accumulations of invertebrate organisms with bedded, eventually massive, lens-like or mound-like geometries embedded in sediments of different compositions (Cumings 1932). In the modern, *Halimeda* bioherms are probably the most representative example of these bioconstructions (Davies 2011).

Halimeda bioherms are described from Holocene marine deposits all over the world, including the Nicaraguan Caribbean Sea (Hine et al. 1988), the Java Sea (Phipps and Roberts 1988), and most notably in the Great Barrier Reef (Orme et al. 1978; Orme and Salama 1988). In the Great Barrier Reef (GBR), *Halimeda* bioherms are larger in size than anywhere else and often associated with an extensive sheet-like form, described as biostromes (Orme and Salama

Published online: 30 May 2024

1988), and surfaces covered by *Halimeda* meadows (Drew and Abel 1988; Wienberg et al. 2010). *Halimeda* meadows are significantly more ubiquitous than mounds, and they have also been described from other carbonate tropical factories such as, for example, for the Great Bahamas Bank (Freile-Pelegrin et al. 1995) and Hawaii (Harney et al. 2000; Harney and Fletcher 2003; Spalding 2012). The majority of these *Halimeda*-rich bioconstructions or meadows are attributed to nutrient-rich waters that provide the nutrients required to enhance the *Halimeda* growth (Wolanski et al. 1988).

The GBR *Halimeda* bioherms were intensely studied (Orme et al. 1978; Orme and Salama 1988; Drew and Abel 1988; Wolanski et al. 1988; Rees et al. 2007; McNeil et al. 2016, 2021a, b). McNeil et al. (2021a, b) proposed three different bioherm morphotypes defined by the surface area, the thickness, and the volume. These parameters provided rough information on the biological and sedimentological mechanisms controlling bioherm morphology. The GBR bioherm morphotypes are annulate, reticulate, and undulate structures (see Table 3 of McNeil et al. 2021a, b).

Hydroacoustic data, seafloor observation, oceanographic data, and discrete sediment sampling during RV SONNE cruise 292 were used to characterize mound-shaped *Halimeda* buildups on the Queensland Plateau in the Coral Sea. This work for the first time presents the morphology, internal structure, and in situ facies distribution of these mesophotic *Halimeda* bioherms and proposes the definition of a new bioherm morphotype. With the growing understanding of *Halimeda* as a determinative carbonate factory (Rees et al. 2007; Castro-Sanguino et al. 2020; McNeil et al. 2022) and its possible disruption with ocean acidification (Robbins et al. 2009; Sinutok et al. 2012), such understanding becomes crucial.

Geological setting

This research focuses on the carbonates of Tregrosse Bank on the Queensland Plateau, offshore NE Australia (Fig. 1). The basement of the Queensland Plateau consists of metasedimentary rocks (Feary et al. 1993) covered by Paleogene syn-rift sediments (Mutter 1977). The subsidence rate for the Queensland Plateau has been calculated to 9–11 cm/1000 yrs (past 5 Ma), with lower rates before ~ 5 Ma (Müller et al 2000). Carbonate platforms on the Queensland Plateau were established during the middle Eocene (Mutter 1977; Betzler et al. 1993).

The carbonate platforms of the Queensland Plateau appear to follow the classical windward–leeward, E–W, inner platform facies asymmetry: shallow water coral reefs grow along the windward edge of the platforms, which protect an open shallow water area. These areas are depressed and have water depths of 50–75 mbsl. Pinnacles and knolls described as living coral heads are scattered around the seafloor of the open lagoons (Orme et al. 1978). These reefs and banks sit on relicts of a larger Miocene carbonate platform which covered ~ 64.000 km^2 (Mutter 1977; Betzler et al. 1993).

The Queensland Plateau lies in the flow of the North Caledonia Jet, which is a branch of the South Equatorial Current (Ganachaud et al. 2014; Kessler and Cravatte 2013). These waters are nutrient poor and exhibit very low primary productivity (Ceccarelli et al. 2013). The wind regime in the Queensland Plateau is dominated by the trade winds, which, as elsewhere, have intensified at 12 Ma (Groeneveld et al. 2017; Betzler et al. 2016). In the Queensland Plateau, trade winds mainly proceed in SE–NW direction, while surface currents flow from the east, mainly related to the North Caledonian Jet (Kessler and Cravatte 2013). The region is affected by tropical cyclones westward passing over the Queensland Plateau (Bloemendaal et al. 2020). Statistical evaluation of cyclone tracks between 1980 and the present shows that cyclone tracks cluster around the Queensland Plateau (Fig. 1B).

Material and methods

Bathymetric mapping

Multibeam data were acquired by means of the hull-mounted Kongsberg EM122 and EM710 of RV SONNE at cruise speeds of 5.5–8 kn over ground with a grid cell size of 1.5 m in the studied areas. Angular sector coverage was 130°–140°, and data were stabilized for roll, pitch, and yaw. Water column sound velocity profiles were obtained by using XSV-02 probes (Lockheed Martin, Sippican Inc.) and CTD measurements (see Betzler et al. 2022 for details). Sound velocity profiles imply that water mass stratification is very homogeneous throughout the Queensland Plateau. The software QIMERA (v2.4.8, QPS software) was used for processing of multibeam data. Bathymetric data were corrected for astronomic tides using tidal predictions of the Australian Hydrographic Office derived via the software AusTides (Australian Hydrographic Office).

Sub-bottom profiles were recorded using the parametric sediment echosounder Atlas Parasound PS70 (mk2, Teledyne Reson) of RV SONNE, with a desired primary high frequency of 18 kHz and a secondary low frequency of 4 kHz. The system was operated in single-pulse mode. Time–depth conversion of Parasound data was done with a sound velocity of 1500 ms^{-1}. Data processing was performed using the software ReflexW (Sandmeier Software) and comprises data editing, compensation for trace header delay, gain adjustment (using automatic gain control), and

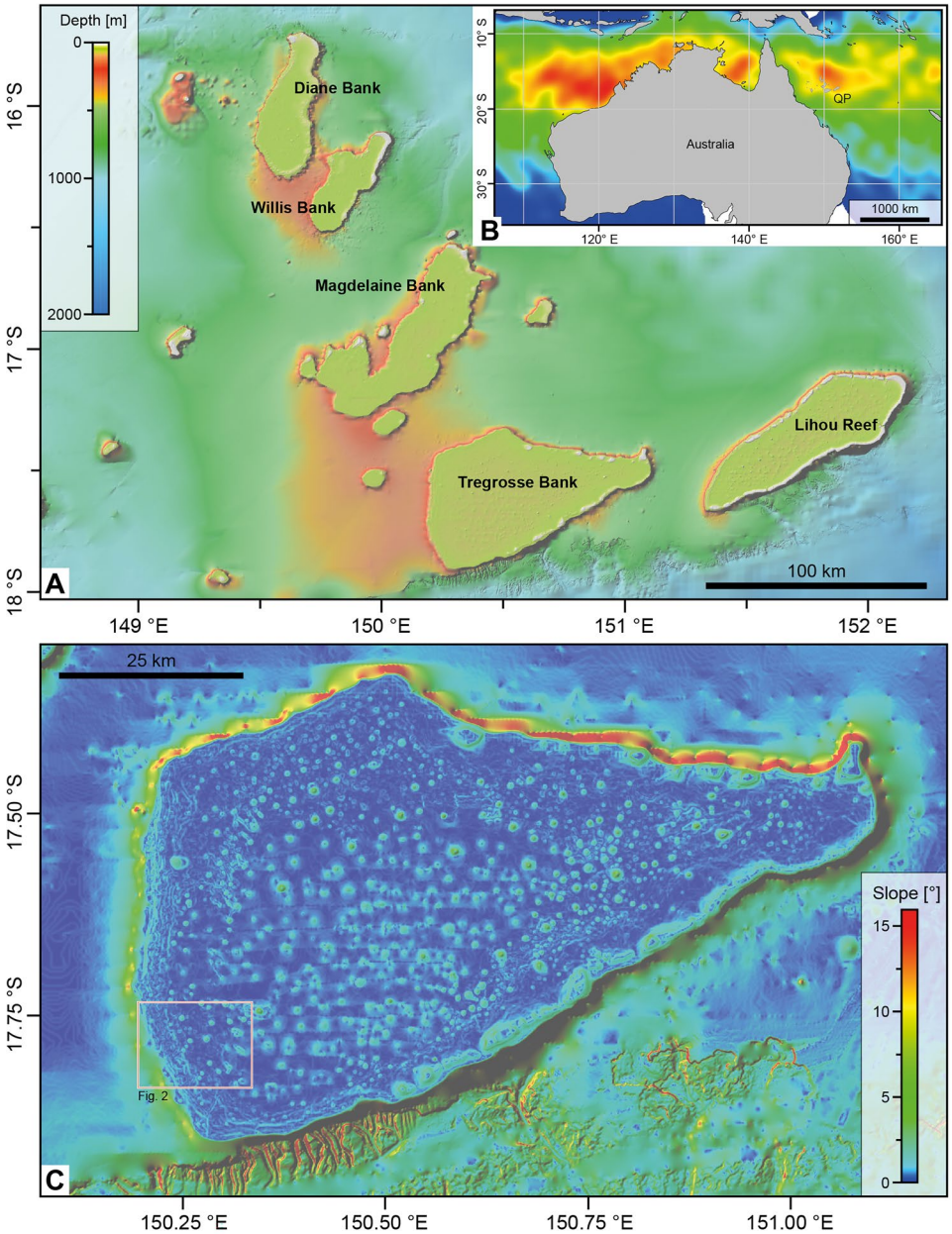

Fig. 1 **A** Large emergent reefs and banks of the Queensland Plateau, northeastern Australia. **B** Cyclone intensity around Australia and the Queensland Plateau (warm colours: strong; blue colours: weak). **C** Slope map derived from bathymetry data of the Tregrosse Bank area. Inset shows Fig. 2 study area

along-profile amplitude normalization. The multibeam bathymetry collected by RV SONNE cruise SO292 was supplemented by Kongsberg EM302 multibeam data collected RV Falkor cruises FK200429 and FK200802 (Beaman 2020).

Sea-floor imaging

During expedition SO292, video observation of the seafloor was performed to image sample locations, to map habitats, and to ground-truth hydroacoustic observations. The Ocean Floor Observation System (OFOS) is a towerable and passively towed frame that includes light, a photo-camera (Canon EOS R5), and a high-definition video camera (Marshal CV350-5X). The system is towed using an 18-mm deep sea fibre-coaxial cable. Compass and an altimeter (Tritech PA500-6) are used to measure the distance between the OFOS and the ocean floor; commonly kept between 3 and 5 m during survey. To scale, equidistant laser dots (40 cm) were projected into the imaged area. The observations of the seafloor based on OFOS data focused on three stations related to three mounds: 09–1 (western bioherm) and 10–1 (eastern bioherm) of the northern transect; and 11–1 for the small bioherms of the southern transect (Fig. 2).

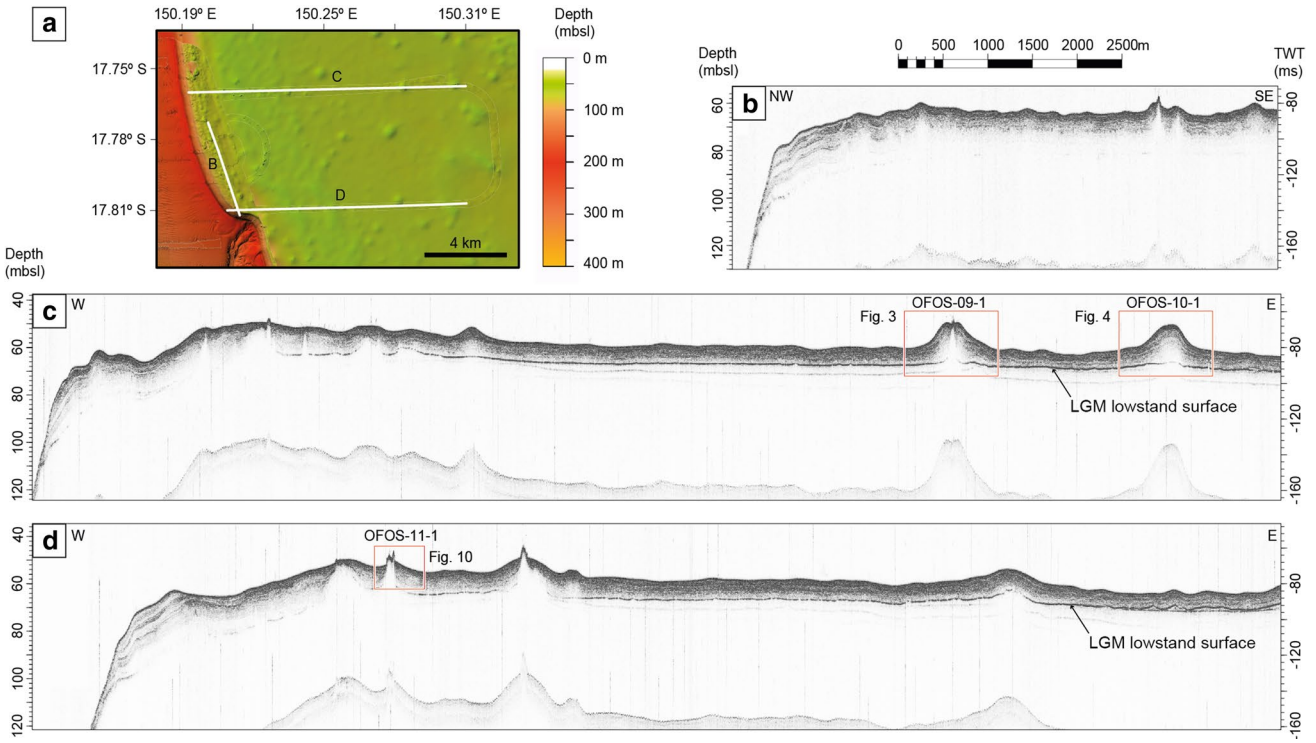

Fig. 2 Parasound profiles of the study area. **A** Bathymetry map with the locations of the Parasound lines at southwestern Tregrosse Bank. **B–D** Parasound profiles with the positions of the studied *Halimeda* mounds. LGM, last glacial maximum

Oceanography

A Sea-Bird 37-SM MicroCAT attached to the frame of the OFOS was used to measure bottom water properties. The MicroCAT features a data logger equipped with a high-accuracy conductivity, pressure, and temperature sensor measuring bottom water conditions. Calibration of the MicroCAT was done at the first CTD station in accordance with the CTD. Logging was set to one sample every 10 s. The pumpless sensor array has been placed approximately 0.5 m above the OFOS altimeter to allow for undisturbed water flow. The RV SONNE is fitted with a self-cleaning monitoring box (SMB) that continuously measures surface water properties using various sensors. The water inlet is located in the bow close to the water line. The SMB is equipped with temperature and salinity sensors (Seabird SBE 45), as well as sensors to measure chlorophyll-a concentration and turbidity (WatLabs FLTNU).

Sedimentology

The top of the Tregrosse Bank was sampled along two east–west transects: one to the north comprising the mounds observed in OFOS stations 09–1 and 10–1; and one to the south corresponding to OFOS station 11–1 (Fig. 2), at water depths between 55 and 71 m. Sea-floor sediment samples were taken by means of box corer (BC). A Box core Imaging System (BOXIS) developed at the Universität Hamburg was mounted on the BC allowing for illuminated high-resolution video recording of the sampled area prior to sampling (GoPro HERO 10, 19 megapixels 5120 × 3840).

All box corer samples were photographed after retrieval (surface and side section) and described. Part of the material was washed over 2 mm, 0.250 mm, 0.125 mm, and 0.063 mm sieves, and dried for later microscopic analysis. The sediment was described following the Dunham (1962) textural classification in conjunction with the depositional textures described by Embry and Klovan (1971). Colour was determined qualitatively using Munsell Soil Colour Charts (Munsell Colour Company, Inc., 2021). Relative abundances of identified components such as mineral grains, microfossils, and biogenic fragments were assigned on a semi-quantitative basis using the following classification: abundant (> 20% of field of view), common (> 5–20% of field of view), few (1–5% of field of view), rare (< 1% of field of view), present (1 per 1–10 fields of view), and barren (none in field of view). The average fields of view were determined under the binocular with magnifications of × 10 for bulk samples and grain sizes larger than 0.250 mm, of × 20 for grain sizes between 250 and 125 mm, and of × 40 for sediment sizes under 0.063 mm. The field of view for smear

slides was determined by the × 200 magnification of the microscope.

Absolute age determination

Absolute ages are based on radiocarbon dating of *Halimeda* flakes. Samples were selected from box core bulk samples. Measurements were done by the MICADAS radiocarbon dating laboratory at the Alfred Wegener Institute in Bremerhaven, Germany (Mollenhauer et al. 2021). Calibration of conventional radiocarbon ages was carried out using the online tool CALIBomb (Reimer et al. 2004; Reimer and Reimer 2004) and the "Great Barrier Reef" post-Bomb calibration dataset (Wu et al. 2021). Calibrated ages are reported as cumulative probability distributions (sigma 2 range) and rounded to the next yr (Table 1).

Results

Platform morphology

Tregrosse carbonate bank is roughly triangular in shape, with its acute angle pointing east. The bank has a surface of 3716 km^2, measured at the 80 m isobath. The bank top is bowl shaped with water depths reaching up to 70 m in the central part. The bank rim is at or above sea level in the eastern and southeastern part; towards the west, it is at a depth of 50–60 mbsl (Figs. 1 and 2). Across the bank interior, there are mound-shaped conical elevations, 3–10 m high above the local baseline and up to 500 m in diameter (Figs. 3, 4 and Table 2). The flanks of the mounds have an inclination from 2° to 5°, with the slopes not being symmetrical (Fig. 1B). These mounded structures also occur at the bank margins, especially along the western platform edge at water depths of 10–70 mbsl, but clustering around 50–65 mbsl. Here, they are smaller compared to the buildups in the bank interior and are often amalgamated (Fig. 2B). At their top, mounds display a small depression, around 100 m wide and less than 1 m deep (Fig. 2C). The central part of this depression may be occupied in some mounds by a smaller pinnacle, which constitutes the highest part of the mounded structures (Figs. 2C, D and 3).

Parasound imagery shows that the sedimentary succession at the top of the Tregrosse Bank has a faint stratification characterized by the alternation of higher and lower amplitude reflections in the interval, overlaying a prominent high-amplitude reflection around 90-ms TWT that hides deeper strata (Fig. 2C and D). c. Five–10 m below the present seafloor (Figs. 3 and 4). The mounds unconformably overlay this strong reflection (LGM in Figs. 2, 3, and 4). Above this reflector, the mounds are characterized by low-amplitude reflections that gradually change, with increasing

Table 1 Calibrated ages for selected samples of the studied *Halimeda* bioherms

Sample								Results				Calibration		
Laboratory ID	Sample ID	Lat (°)	Lon (°)	Water depth (m)	Depth (mbsf)	Material	Weight (µgC)	^{14}C counts	$^{13}C/^{12}C$ (‰)	$_{F}14_{C}$	Conv. age (yrs. BP)	Range (sigma 2 cum.) (yrs. cal. BP)		Prob. distr.
11781.1.1	SO292_21-1_10A	17° 45.503'	150° 17.207'	58	0.10	*Halimeda* flakes	990	492.068	1.0986 ± 1.2	0.9714 ± 0.0026	233 ± 22	−11	−9	1.000
11782.1.1	SO292_21-1_10B					*Halimeda* flakes	1018	484.979	1.0981 ± 1.1	0.9621 ± 0.0026	310 ± 22	−10	3	1.000
11783.1.1	SO292_20-1_15A	17° 45.437'	150° 18.360'	55	0.15	*Halimeda* flakes	1021	538.532	1.0976 ± 1.2	1.0840 ± 0.0029	−648 ± 21	−57	−17	1.000
11784.1.1	SO292_20-1_15B					*Halimeda* flakes	990	544.730	1.0970 ± 1.2	1.1170 ± 0.0030	−889 ± 21	−49	−20	1.000

Calibration by CaliBomb (Reimer et al. 2004; Reimer Reimer, 2023) using "Great Barrier Reef" post-bomb calibration dataset (Wu et al. 2021).

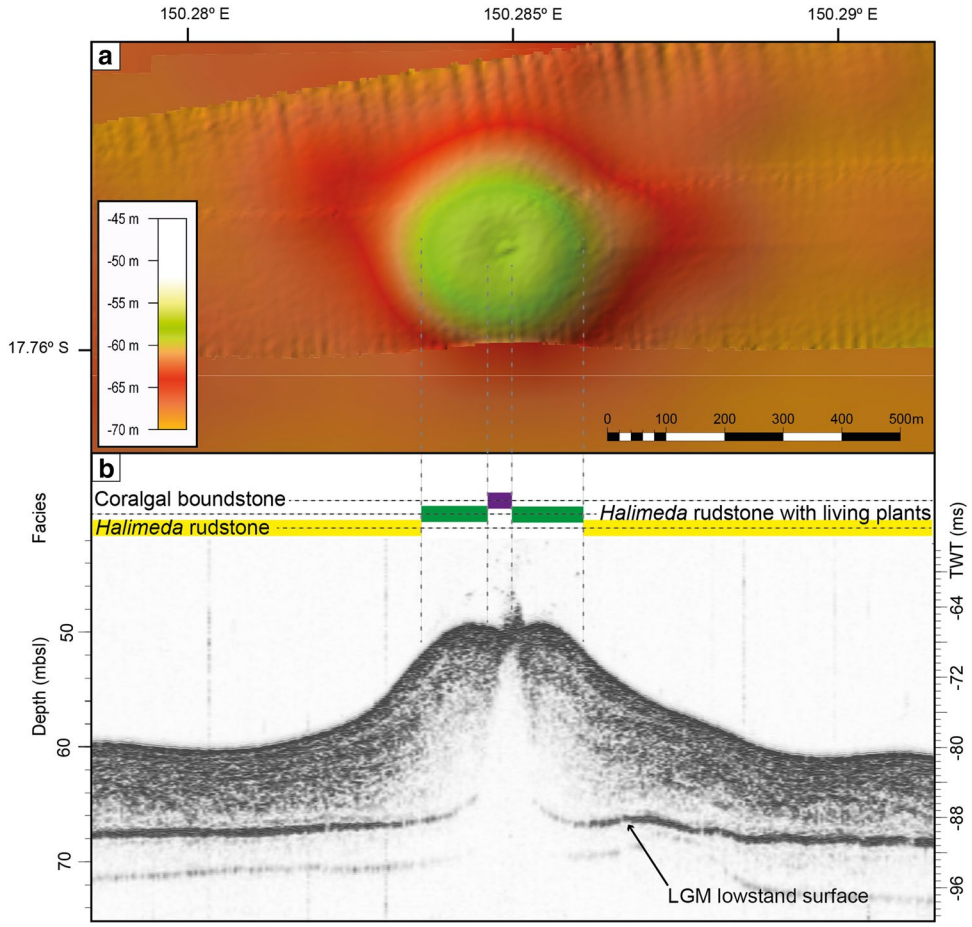

Fig. 3 Profile Bioherm West (OFOS station 10–1). **A** Multibeam bathymetry map. **B** Parasound profile with surface facies distribution. LGM, last glacial maximum

distance from the mound core, into the background high-amplitude reflections of the platform (Figs. 3 and 4). The platform bedding is imaged by high-amplitude reflections that are persistent along the platform transects and only display an interdigitation with weaker reflections in the flanks of the mounds. This alternation and interfingering of low- and high-amplitude reflections within the mounds resemble a "Christmas tree"-like structure (Figs. 3 and 4) and present a west–east asymmetry, with slightly steeper flanks towards the east (Fig. 4).

Water mass properties

Data on water mass properties were gathered for OFOS stations 09–1, 10–1, and 11–1 (Table 3). Less than 12 h passed between all measurements. The surface water temperature at all locations remained similar over the observation period (27.1 ± 0.05 °C). Surface water salinity was 34.86 ± 0.005 PSU. Surface turbidity was 0.181 ± 0.005 NTU, i.e. the surface water was very clear. The near-seafloor temperature adjacent to the mounds was 26.5 ± 0.12 °C, and salinity was 35.13 ± 0.033 PSU. Water temperature of the platform at comparable depths (50–70 mbsl) was 25.1 ± 0.25 °C and salinity 35.35 ± 0.032 PSU.

Light data collected around the platform exhibit uniform trends. Fitting the data yields an extinction coefficient of $4.76 \pm 0.04 \times 10^{-2}$ with photosynthetic available radiation (PAR) declining to 4% at a depth of 50 m and to 1% at 80 m.

Sedimentology

Platform facies

The dominant facies on the plain of the inner platform of the Tregrosse Bank, which we regard as the background facies, consists of an unconsolidated bioclastic rudstone with abundant *Halimeda* plates. There is variability on the surface distribution of some components within this *Halimeda* rudstone likely due to the patchy distribution of bryozoan–sponge nodules over the background gravel of *Halimeda* plates (Fig. 5A–C). The patches of nodules are darker in colour with respect to the background white sediment and are irregular in size, ranging between 1 and 7 cm. The patches are arranged in larger clusters between 20 and 100 cm in size (Fig. 5B), with a greater elongation

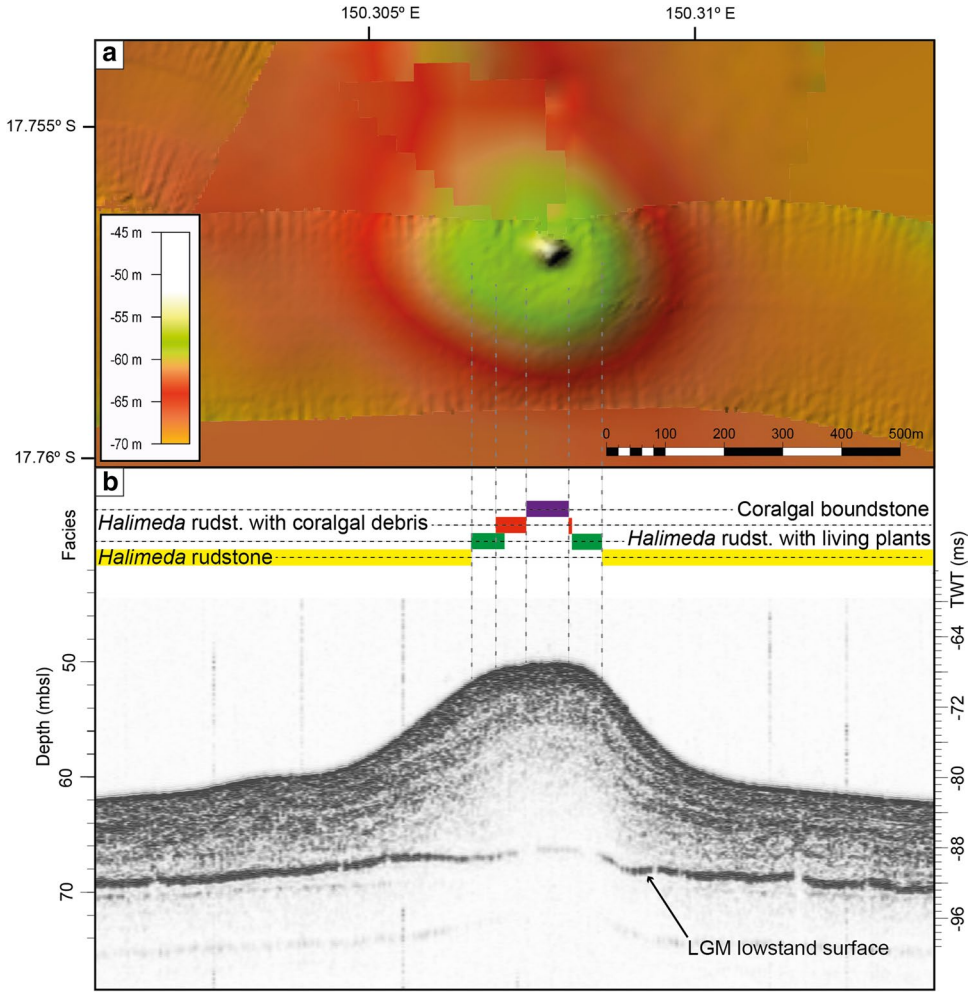

Fig. 4 Profile Bioherm East (OFOS station 09–1). **A** Multibeam bathymetry map. **B** Parasound profile with surface facies distribution. LGM, last glacial maximum

Table 2 Main features of the new *Halimeda* bioherm morphotype from the Queensland Plateau (Coral Sea, Australia)

Depth range (top of mound) (mbsl)	10–70 (average 50–65)
Diameter (m)	< 500
Elevation (m)	3–10
Flank inclination (°)	2–5
Surficial structure	1–4 facies belts
Internal structure	Aggrading low-amplitude reflections (mound core material) interfingering with high-amplitude reflections (platform material)

in NE–SW direction. The stained nodule clusters display a reticulate pattern because of the abundant bioturbation. The bioturbation mostly consists of deep depressions, up to 30 cm wide and surficial elongated structures. Locally, the accumulations of nodules occur in the surrounding of scattered living *Halimeda* plants.

Main components of the rudstone are *Halimeda* plates (more than 85% on average), followed by coralline red algae, common to few large benthic foraminifera (*Sorites*, *Heterostegina*, *Alveolinella, and Amphistegina*) as well as encrusting *Homotrema*, coral fragments (commonly encrusted by coralline red algae), bryozoans, and rare to present echinoid remains and mollusk fragments. Living echinoids, sea-urchins, starfishes, and sea cucumbers are locally abundant at the seafloor. However, very few fish were observed here or in any other location through the survey. The *Halimeda* plates range in size between 2 and 15 mm. They usually occur as individual pristine flakes (Fig. 5D and E), but they can also present bryozoan–sponge coatings that may agglutinate few plates in living position or in nodules of up to 3 cm (Fig. 5F).

Table 3 Water properties around the studied *Halimeda* bioherms of the Tregrosse Bank

	OFOS-09–1	OFOS-10–1	OFOS-11–1
Surface water			
Temperature (°C)	27.1	27.1	27.1
Salinity (PSU)	34.8	34.8	34.9
Turbidity (NTU)	0.18	0.18	0.18
Chlorophyll (µg chl-a/l)	0.08	0.08	0.06
Bottom water			
Depth (mbsl)	55.0	55.6	54.2
Temperature (°C)	26.6	26.4	26.5
Salinity (PSU)	35.1	35.1	35.1

Towards the western edge of the Tregrosse Bank, the prevalence of living plants increases. In this area, the living *Halimeda* algae, in situ growing plants, at the seafloor for a reticulate pattern enclosing 40–75 cm wide depressed areas with *Halimeda* gravel (Fig. 6A). The preservations of the in situ growing *Halimeda* changes from completely green individuals to others with lighter-coloured plates with eventual crusts of sponges, bryozoan, and red algae (Fig. 5), and other brown-coloured coatings likely formed by algal mats (Fig. 6B). Larger benthic foraminifera are common, especially of the genus *Sorites,* in this area reaching diameters of up to 4 cm. Bryozoan and sponges can be locally abundant. Bioturbation is intense in the pockets with *Halimeda* rudstone.

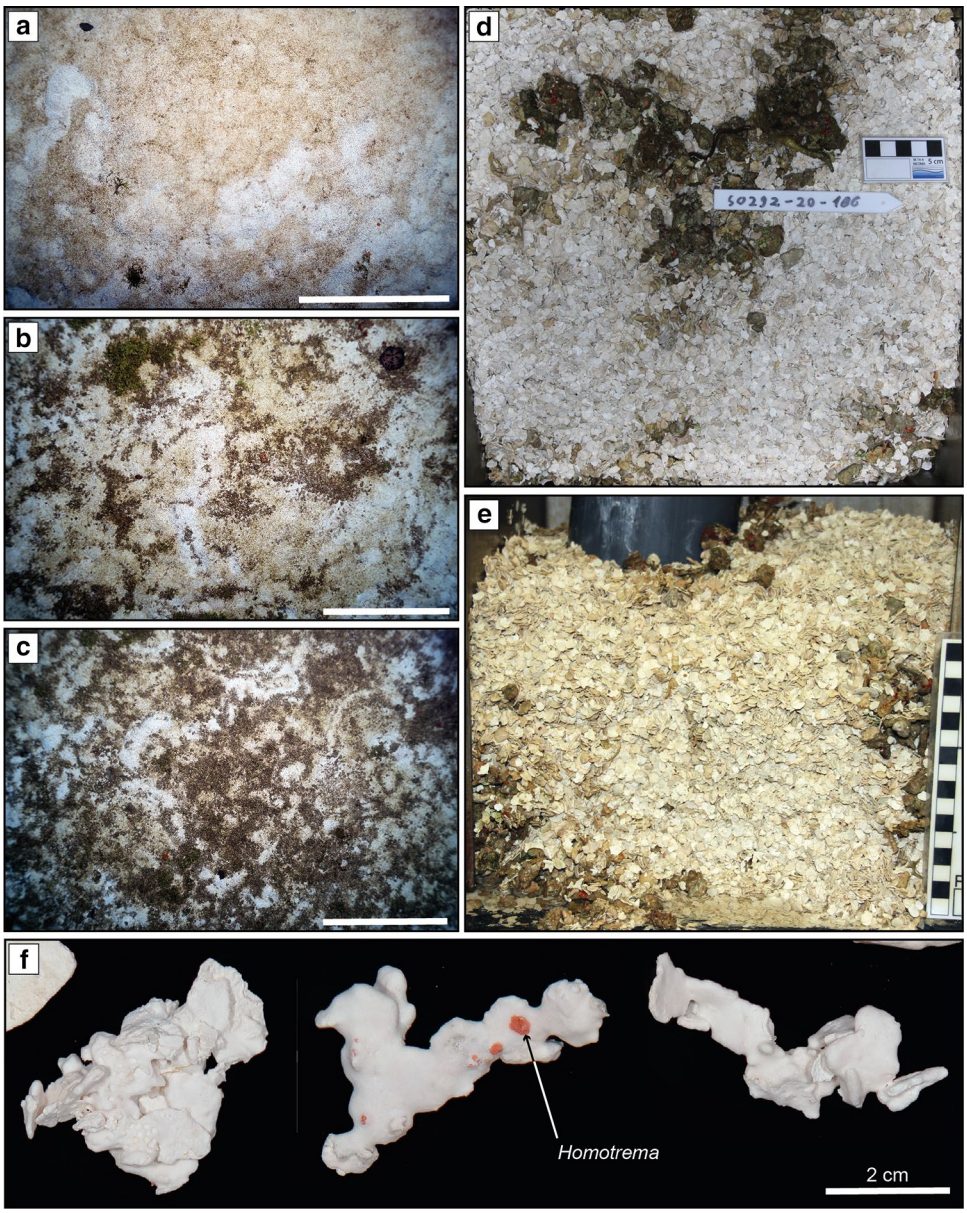

Fig. 5 *Halimeda* rudstone (OFOS station 09–1). **A–C** Surface variability in the amount of stained coated grains (mostly sponges and bryozoan) on the seafloor surface. Scale bar 1 m. **D** Close-up of the surface retrieved by a box corer on the *Halimeda* rudstone (SO292_20-1BC). Darker material is encrustations of sponges and bryozoans. **E** Sediment retrieved by box corer on the *Halimeda* rudstone. **F** Colonial foraminifera *Homotrema* encrustations on *Halimeda* segments

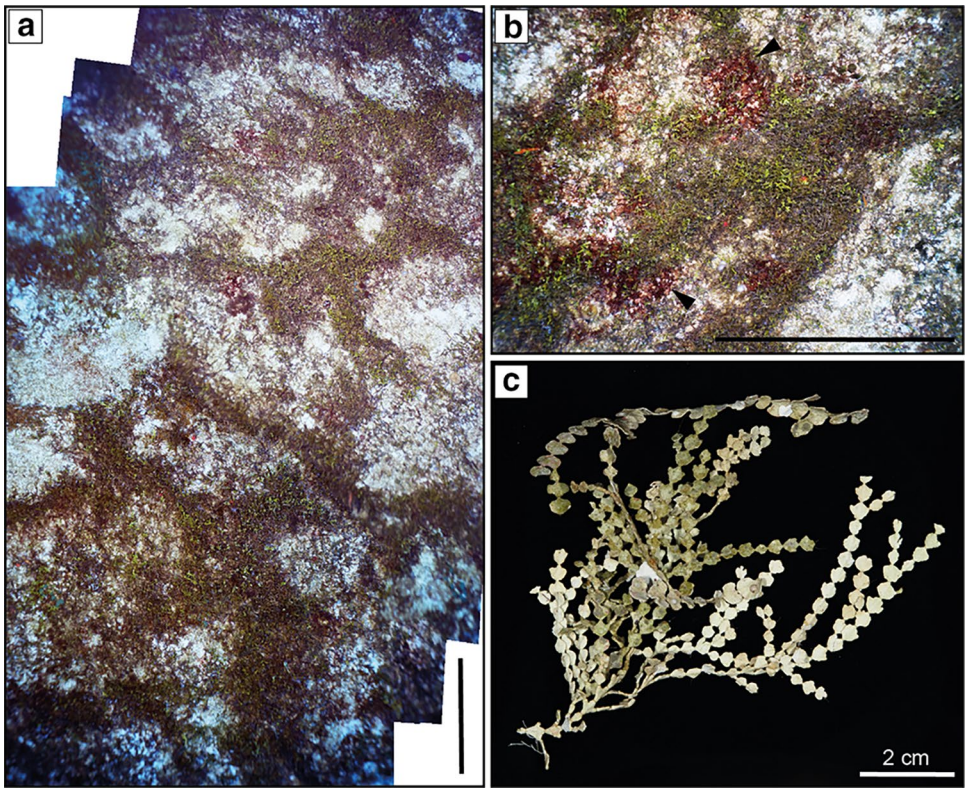

Fig. 6 Occurrence of *Halimeda* at depth of 60 mbsl (OFOS station 10–1, Fig. 3). **A** Patchy distribution of brown–green-coloured living *Halimeda* plants amongst white-coloured dead *Halimeda* rudstone. Scale bar 1 m. **B** Algal mats (black arrowheads) amongst *Halimeda* plants. Scale bar 1 m. **C** Example of articulated dead *Halimeda* plant. Note the colour loss as pigments leach from the segments towards the base

The *Halimeda* rudstone facies, with its local variability, occupies the majority of the observed Tregrosse Bank, except for the mounded structures observed in the multibeam bathymetry (Figs. 3 and 4). The mounded structures are also dominated by *Halimeda* facies but display a significant facies variability in contrast with the Halimeda rudstone of the background platform facies.

Halimeda mounds

Based on the direct sea-floor observations with the OFOS and the discrete samples retrieved by the BC, the mounds can be subdivided into four surface facies belts including from deepest to shallowest: (1) *Halimeda* rudstone, (2) *Halimeda* rudstone with living plants, (3) *Halimeda* rudstone with coral and coralline red-algae debris, and (4) coralgal boundstone. The diverse facies in the *Halimeda* mounds are documented in Table 4. Facies distribution is shown in Figs. 3 and 4.

The *Halimeda* rudstone reaches the lowermost part of the mounds where it gradually changes into a facies marked by the presence of living *Halimeda* plants. The amount of living *Halimeda* increases from the base of the mound to the top of this facies belt. The plants are commonly around 30 cm in size and commonly occur in clusters up to 2 m wide (Fig. 7A). This facies also shows other living green algae such as *Dictyospheria* (Fig. 7B). Together with *Halimeda,* there are LBF represented by *Cycloclypeus* and *Sorites* (Fig. 7C), which were also observed living on the *Halimeda* plants as epiphytes. *Sorites* individuals range in size between 0.5 and 2 cm and are also a major component of the sediment below the plants (Fig. 7C and Table 4), together with pristine *Halimeda* flakes, and plates with bryozoan–sponge coatings that may agglutinate few plates in living position or in nodules of up to 3 cm. Encrusting foraminifera *Homotrema*, bryozoan, and minor serpulids also colonize the *Halimeda* plates (Fig. 7D). Towards the upper part of this facies belt, there may be a progressive increase in the amount and size of coral debris encrusted by red algae, which constitutes the transition zone to the next facies belt, the *Halimeda* rudstone with coral/red algae debris (Figs. 4, 5, 6, and 7E).

The main feature of the *Halimeda* rudstone with coral/red algae debris facies belt is the abundance of coral rubble, mainly encrusted by red algae, constituting between 60 and 97% of the sea-floor surface. There is a patchy distribution of the debris in this facies belt, but as a general trend, the amount and size of the debris increase towards the top of the mounds (Fig. 8A). The areas with higher amount of encrusted coral debris constitute pavements where bioturbation is rare (Fig. 8B). In the areas with minor debris, there are common living *Halimeda* plants and medium to intense bioturbation that allows for the recognition of the underlying white *Halimeda* rudstone (Fig. 8C and D). *Halimeda* plants are smaller and less abundant compared to the other

Table 4 Surface facies of the *Halimeda* bioherms of the Queensland Plateau

Facies name	Surface description	Sand/gravel composition	LBF assemblage	Matrix (< 63)	Position/extension
Halimeda rudstone	White Halimeda sands/gravels intensely bioturbated with darker nodule patches (0–75% of seafloor surface)	Halimeda (96.5%), LBF (1.5%), gastropods (0.5%), and sponges (0.5%). Minor: coral, red algae, bivalves, bryozoan, and unidentifiable bioclasts	Sorites (43%), Calcarina (38%), Heterostegina (16%), and Alveolinella (3%)	Sponge spicules, ascidian spicules, planktic foraminifera fragments, and unidentifiable bioclasts	Platform/distal part of the mound. Hundreds of metres
Halimeda rudstone with living plants	White Halimeda sands/gravels with abundant living Halimeda plants (40–79 of seafloor surface) and nodule patches. Plants locally bearing large benthic foraminifera Sorites. Some bioturbation	Halimeda (94%), LBF (3%), coral and red algae (0.5%), gastropods (0.5%), bryozoan (0.5%), and sponges (0.5%). Minor: coral, red algae, bivalves, unidentifiable bioclasts, and present ostracods	Sorites (45%), Heterostegina (40%), Alveolinella (12%), and encrusting foraminifera Homotrema (3%)	Unidentifiable bioclasts, sponge spicules, ascidian spicules, planktic foraminifera fragments, and quartz	Lower half of the mound.120 m–60 m wide rim
Halimeda rudstone with coralgal debris	Accumulation of coralgal debris from patches (37%) to a reddish pavement (94%) covering the Halimeda gravel. Little bioturbation	Halimeda (87%), LBF (3%), coral and red algae (2%), and unidentifiable bioclasts (4%) Minor: benthic foraminifera (1.5%), bryozoan (1%), gastropods (1%), and present bivalves, echinoids, and sponges	Sorites (20%), Calcarina (20%), Amphistegina (18%), Alveolinella (14%), Heterostegina (3%), and encrusting foraminifera Homotrema (25%)	Sponge spicules, ascidian spicules, planktic foraminifera fragments, and unidentifiable bioclasts	Upper half of the mound (where present). Around 50 m wide rim
Coralgal boundstone	Living platy corals and in situ accumulation of coralgal debris (98% of seafloor surface). Few living Halimeda plants	Halimeda (63.5%), LBF (9%), coral and red algae (8%), and unidentifiable bioclasts (12%) Minor: echinoids (2%), bryozoan (1.5%), gastropods (1%), benthic foraminifera (1%), and present pteropods and sponges	Sorites (28%), Calcarina (17%), Amphistegina (17%), Operculina (7%), Heterostegina (3%), and Alveolinella (1%). Encrusting foraminifera Homotrema (21%)	Sponge spicules, ascidian spicules, planktic foraminifera fragments, unidentifiable bioclasts, and quartz	Top of the mound (where present). 75 m–40 m wide area

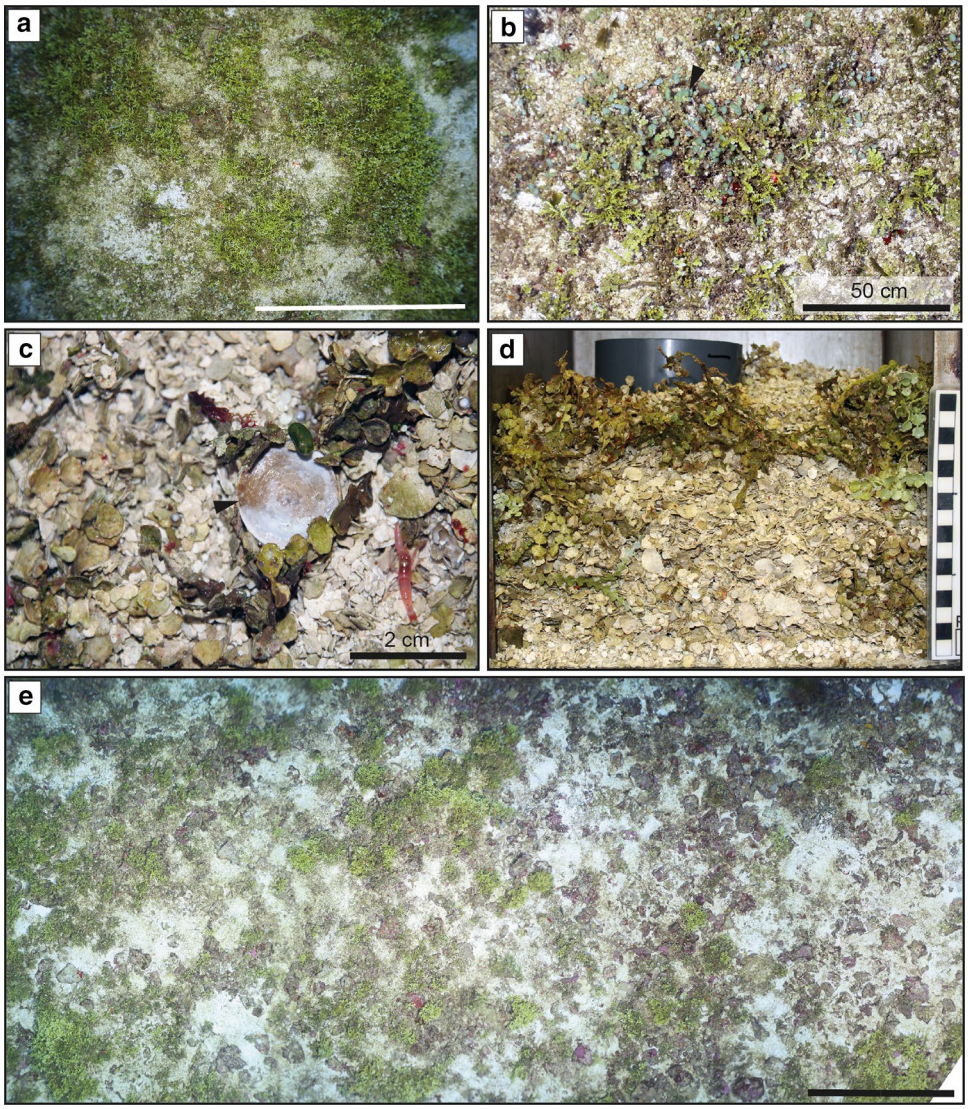

Fig. 7 *Halimeda* rudstone with living plants at depths between 52 and 51 mbsl (OFOS station 09–1, Fig. 4). **A** Cluster of living *Halimeda* plants. Scale bar 1 m. **B** Close-up of the seafloor at SO292_17-1BC showing the green algae *Dictyospheria* (black arrowhead) amongst the living *Halimeda*. **C** Large benthic foraminifera *Cycloclypeus* (black arrowhead) amongst the *Halimeda* plates from SO292_17-1BC. **D** Sediment retrieved by box corer on the *Halimeda* rudstone with living *Halimeda* plants. **E** Transition zone from the *Halimeda* rudstone with living plants to the *Halimeda* rudstone with coralgal debris. Scale bar 1 m

facies belts. In some mounds, as at OFOS station 10–1, this facies belt does not occur or is combined with the coralgal boundstone at the top of the mound (Fig. 3).

The coralgal boundstone occupies the highest and central part of the mounds (Figs. 3 and 4). It consists of abundant living encrusting and platy corals surrounded by coralgal debris (Fig. 9A–C). Amongst the debris, there are sediment patches that consisted of *Halimeda* rudstone with an increased number of sand-sized fragments of corals and red algae with respect to the other facies belts (Fig. 9D and Table 4). Most of the corals ranges in diameter between 15 and 40 cm, but some of them may reach more than 1 m (Fig. 9B). The coral assemblage is dominated primarily by *Pachyseris speciosa* and secondarily by *Podabacia crustacea* (Fig. 9E). Branched bryozoan, sponges, anemones, and sea feathers can be locally common. Fishes are abundant in this part of the mound and may be bioturbated the sediment below the platy corals (Fig. 9B). Some mounds do not present this central part occupied by a coralgal boundstone, and they consist of the flanks to the top of *Halimeda* rudstone with living plants facies (Fig. 10).

Depositional ages

Four samples containing clean *Halimeda* flakes were selected for absolute age determination from the two box cores SO292_20-1 and SO292_21-1. Sampled depths were 0.15 m and 0.10 m below the seafloor for cores 20–1 and 21–1, respectively (Table 1). Conventional radiocarbon ages range between 310 and −889 yr BP ($F^{14}C$ 0.9621 to 1.1170) and are, therefore, too young for the standard marine calibration dataset which requires a minimum conventional radiocarbon age of about 600 yr (Stuiver and Reimer 1993; Heaton et al. 2020). Post-bomb calibrated ages range between −57 and 3 yr BP and are, therefore, regarded as recent,

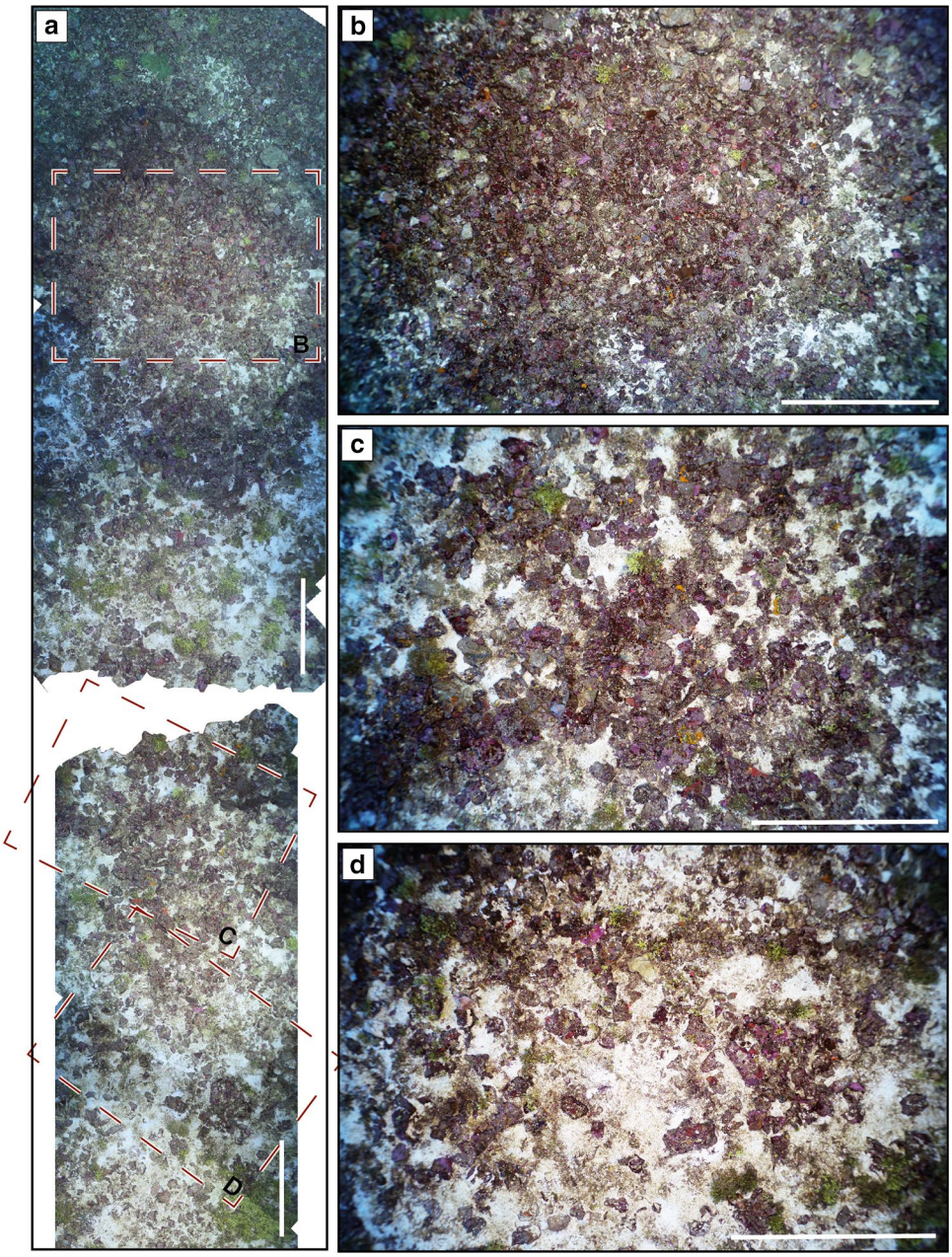

Fig. 8 *Halimeda* rudstone with coralgal debris at depths between 51 and 50 (OFOS station 09–1, Fig. 4). **A** Transect across the coralgal debris facies belt. Scale bar 1 m. Top of the bioherm is at the top of the picture. Dashed areas show the relative abundance of coralgal debris from **B** pavement of coralgal debris to **C** abundant, and **D** common coralgal debris on white *Halimeda* rudstone

pointing to a high grade of post-depositional sediment mixing, at least in the upper decimetres of the sediment column.

Discussion

A new type of *Halimeda* bioherm

Elevating up to 10 m over the surrounding seafloor, with diameters of hundreds of meters, and constituted mostly by in situ accumulations of skeletal grains, mostly of *Halimeda*, the prominent mound structures on top the Tregrosse Bank (Table 2) can be referred to as bioherms (sensu Cumings, 1932). Their surficial facies distribution, with an apex dominated by mesophotic coral reefs in most of the cases (Table 4), makes the *Halimeda* mounds of the Queensland Plateau sensibly different to any other Holocene/modern *Halimeda* bioherm in the literature. Some of the differences with respect to other *Halimeda* mounds descriptions in the literature might be attributed to differences in data resolution between older studies (coarser resolution) and this study (high resolution, especially with respect to direct seafloor observations). However, there are features as depth of occurrence, thickness or internal structure obtained from geophysical data that are directly comparable to other Holocene/modern *Halimeda* mounds elsewhere (Table 5). Thus,

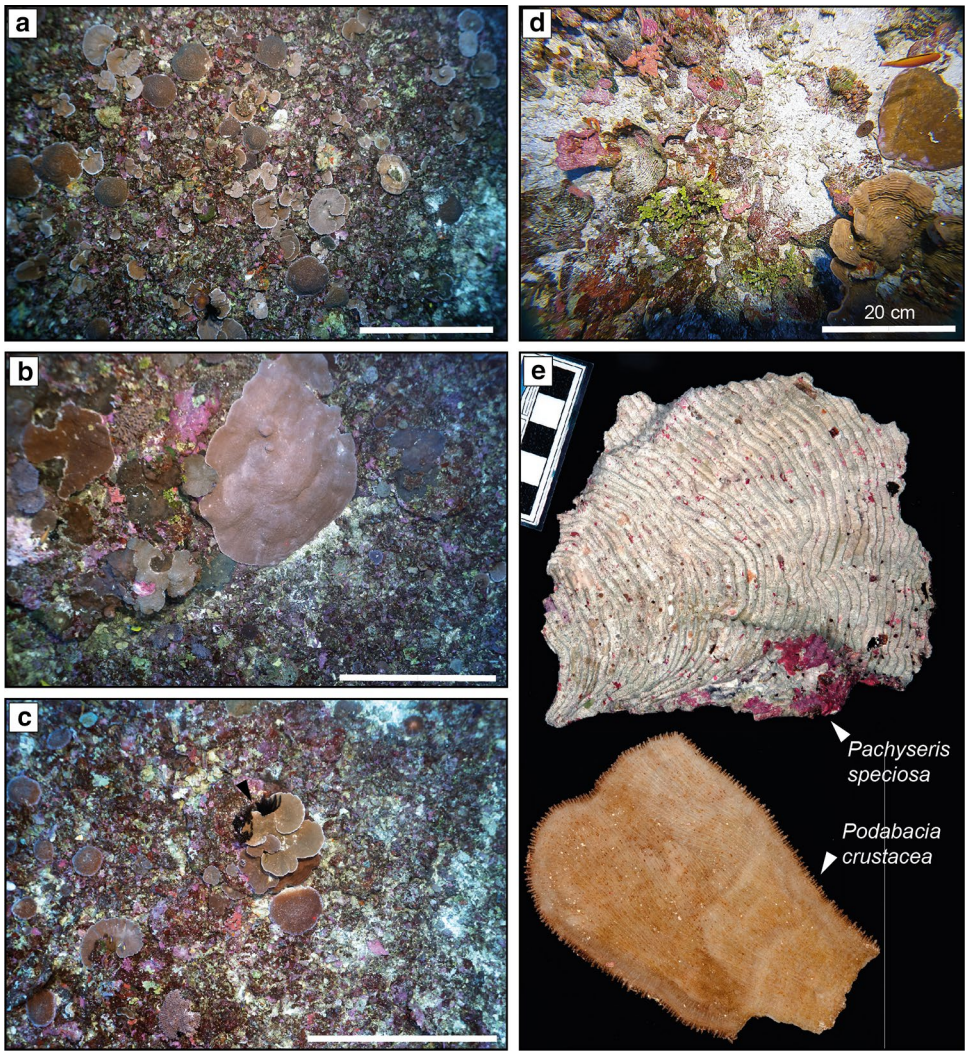

Fig. 9 Coralgal boundstone at depth of 50 m (OFOS station 09–1, Fig. 4, and SO292_18-1BC). Scale bars 1 m. **A** Boundstone facies in the central part of a bioherm. **B** Close-up of large platy coral Pachyseris speciosa. **C** Corals of different sizes and morphologies and feather stars (black arrowhead). **D** Coralgal boundstone facies captured by the box corer camera at station SO292_18-1BC. **E** Close-up of the two main species of corals recovered by the box corer

accordingly to their depth of occurrence and their internal structure, with interfingering of low- and high-amplitude reflections in Parasound profiles, the *Halimeda* mounds of the Queensland Plateau are unique with respect to the rest of *Halimeda* bioherms (Table 5).

There are different modes of growth for *Halimeda* bioherms. Outcrop studies of *Halimeda* bioherms have unravelled the internal structure of such bodies, with a focus on *Halimeda* bioherms of the Miocene of South Spain (Braga and Martín, 1996; Martín et al. 1997) or recently the Oligocene *Halimeda* buildups of the South China Sea (Fournier et al. 2024). These Miocene bioherms are considered comparable to modern examples with respect to biota, lateral extension, and depositional depth (Martín et al. 1997). The internal architecture of the bioherm includes three main elements: (1) a coral framework core; (2) a thick *Halimeda* rudstone cover; and (3) a bioclastic–microbial cap facies. These facies belts wedge out into flank facies consisting of calcarenite made up of mound-derived material (Martín et al. 1997). However, the coral framework in these mounds is exclusively occurring at the base of the mound and covered by the rest of facies (Martín et al. 1997); in contrast with the bioherms of the Queensland Plateau in which the coralgal boundstone occurs at the top surface of the mound and laterally interfingers with the *Halimeda* dominated facies (Figs. 3 and 4).

In modern-day euphotic/upper mesophotic examples of the Great Barrier Reef, recurring phases of growth of *Halimeda* alternate with intervals of growth interruption. It was proposed that during these interruptions, algal mats overgrow the *Halimeda* gravel and stabilize the surfaces of the bodies (McNeil et al. 2021a, b). This has been suggested as the main mechanism for the development of the different morphotypes of bioherms and the bedded internal structures observed in high-resolution seismic data at the Great Barrier Reef (McNeil et al. 2021a, b).

In the herein studied examples, there is no evidence of significant microbial binding in any sample collected from the surface of the bioherms. The presence of algal mats is very limited and restricted to specific areas of the *Halimeda*

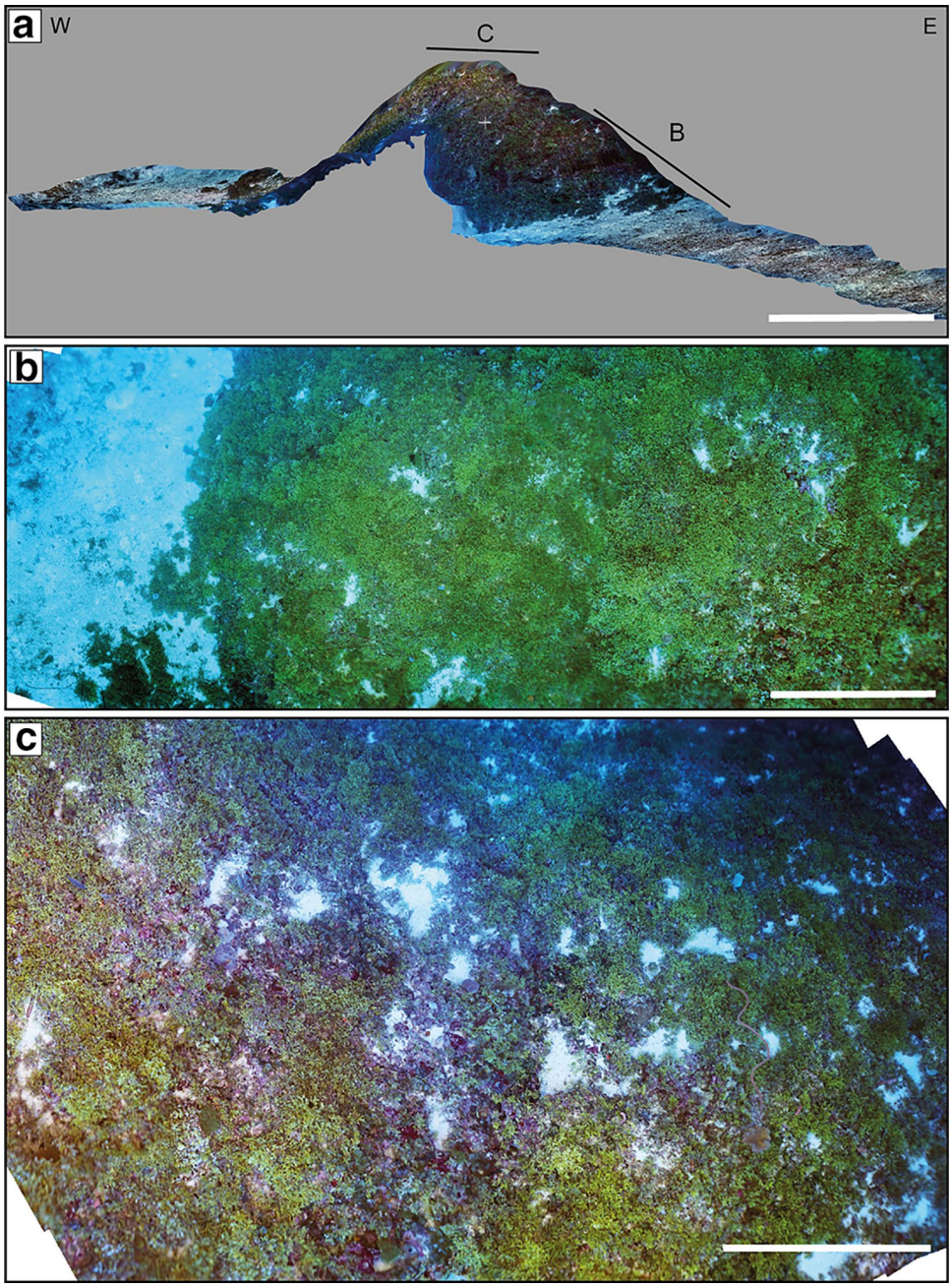

Fig. 10 *Halimeda* bioherm (OFOS station 11–1). **A** Photogrammetric model of the bioherm covered by living *Halimeda* plants. Scale bar 5 m. **B** Panorama of the toe of the bioherm with the transition from living *Halimeda* plants, green, to *Halimeda* rud- stone, white-coloured platform sediment. **C** Panorama view of the top of the bioherm. Scale bar 1 m

rudstone surrounding the bioherm (Fig. 6B). In the samples retrieved on the bioherms, some evidence of early lithification is present, mainly by encrusting sponges, bryozoan, and red algal crusts (Fig. 5F). The bioherms of the Queensland Plateau do not show convex-up parallel bedding as their counterparts on the Great Barrier Reef, but rather record convex-up lens-like reflections that wedge out towards the bioherm flanks alternating with laterally more continuous sediment packages (Figs. 3 and 4). We propose that this alternation is the result of two processes: accumulation of *Halimeda* debris and the episodic dismantling of the mesophotic coralgal boundstone at the centre of the bioherm.

The mesophotic corals might be periodically affected by currents, for example, triggered by severe storms that partially dismantle living corals at the top of the bioherms and export coralgal rubble to the flanks. During fair-weather periods, *Halimeda* likely recolonize the flanks partially or completely covering (Fig. 10) the coralgal debris belt. This alternation of intervals dominated by coral debris with intervals dominated by *Halimeda*, gravel, may explain the interfingering between low-amplitude and high-amplitude reflections imaged in the Parasound profiles (Figs. 3 and 4). Low-amplitude reflections would represent large extension of coralgal debris, while high-amplitude reflections stand for

Table 5 Holocene/modern *Halimeda* buildups morphotypes of the Java Sea, Nicaragua, Hawaii, Great Barrier Reef "GBR," and Coral Sea (Australia) and their characteristic (modified from McNeil et al., 2021a, b)

Halimeda buildups morphotype	Description	Average depth (mbsl)	Thickness (m)	Average inclination	Internal structure
Eastern Java Sea (Roberts et al. 1988)	Low relief near symmetrical semi-spherical elevations (haystack shape), commonly amalgamated	20–40	20–50	–	Planar- slightly convex-up parallel reflections
Nicaragua mosquito channel (Hine et al. 1988)	Pinnacles around 20–30 m high with lateral extension of up to 200 m	40–50	20–40	–	Chaotic-transparent seismic facies with a lens or pod-like geometry in cross-section
Hawaii mounds (Spalding 2012)	Low relief (up to 0.25 m) and up to 100 m^2	ca. 50	0.25	–	–
GBR reticulate (McNeil et al., 2021a, b)	High relief, irregular sharp sinuous crests, complex honeycomb rugosity, non-circular	24.52	5–20	1.88°	Planar-slightly concave-up parallel reflections with eventual truncation
GBR annulate (McNeil et al. 2021a, b)	Circular ring shapes, hollow centred with or without central pinnacle, often coalescing together	28.64	5–20	2.71°	Planar- slightly convex-up parallel reflections
GBR undulate (McNeil et al. 2021a, b)	Sinuous and wave-like, smooth crests, with low relief above surrounding sediment	25.67	5–20	1.38°	Planar parallel reflections
This work	Conical elevations with gentle slopes, a small depression, around 100 m wide and less than 1 m deep at their top. The central part of the depressions may be occupied by a small pinnacle	50–65	3–10	2.5°	Aggrading low-amplitude reflections (core material) interfingering with high-amplitude reflections (platform material)

the flank overgrowth by *Halimeda* plants. Mounds where the coralgal boundstone facies are missing also lack the interfingering of low-amplitude and high-amplitude reflections in the Parasound profiles (Fig. 2). This is probably because after a first dismantling event (i.e. a storm), corals were not able to recover, and the mound was fully overgrown by *Halimeda*, which is consistent with the homogeneous acoustic facies imaged in the Parasound profiles (Fig. 2) and the direct observations with OFOS (Fig. 10).

Origin of the bioherms: exposure, reflooding, and coral growth

All the bioherms of the Tregrosse Bank have their bases on minor elevations of a distinct surface that can be traced in all Parasound data (Fig. 2). It is proposed that this surface likely traces the surface of emersion which formed by subaerial platform top exposure during lower sea-level conditions, likely during the Last Glacial Maximum (LGM, Yokoyama et al. 2018). An equivalent surface is reported at the Great Barrier Reef, where McNeil et al. (2021a, b) interpreted it as a Pleistocene erosional unconformity that marked the substrate of the Holocene *Halimeda* bioherms (Reflector A of McNeil et al. 2021a, b).

The proposed lowstand surface is at deeper position at Tregrosse Bank, 90 ms in TWT, in contrast with 50 ms in the GBR (McNeil et al. 2021a, b). Ninety milliseconds would be equivalent to a depth of ~ 70 mbsl, around 5–10 m below the seafloor, assuming a sound velocity of 1500 ms^{-1} in the sediment. This would imply that the flooding of the Tregrosse Bank interior was during the rapid sea-level rise at the beginning of the late glacial interstadial, around 14 kyr ago (Lewis et al. 2013; Yokoyama et al. 2018).

Corals growing on the formerly exposed basement substrate during this mid-deglacial flooding likely formed patch reefs, possibly in euphotic conditions (Fig. 11). These elevations could have formed the nucleus for subsequent bioherm development. With the progressive sea-level rise, the euphotic coral assemblage was replaced by a mesophotic coral assemblage that still persists nowadays. We propose that aggradation and dismantling of euphotic to mesophotic reefs was the main growth mechanism during the first stages of bioherm development.

The mesophotic corals at the centre of the bioherms

With respect to the corals constituting the core of the bioherm today, *Pachyseris speciosa* (Fig. 9E) is the second-most recorded species in mesophotic reefs of the Indo_Pacific realm (Turak and DeVantier 2019). This coral typically forms large beds of foliose to platy morphology in bottoms with low-light conditions (Chow et al. 2019; Turak and DeVantier 2019). *Pachyseris* displays platy growth forms, as in the studied bioherms, oriented to optimize light capture (Iwase et al. 2008; Turak and DeVantier 2019). This platy morphology may be critical to their success in this setting as it makes the coral less susceptible to algal encroachment (Hughes 1989; Tanner 1995). Their presence in the Queensland Plateau is consistent with their biogeographical distribution in the adjacent Great Barrier Reef and Solomon Islands, where they are the main coral species in the mesophotic reefs (Chow et al. 2019; Turak and DeVantier 2019). In these areas, *Pachyseris* occurs in the upper mesophotic zone (30–60 m), with a certain preference to rubble–sand substrates and small blocks (Turak and DeVantier 2019) and water temperatures between 24 and

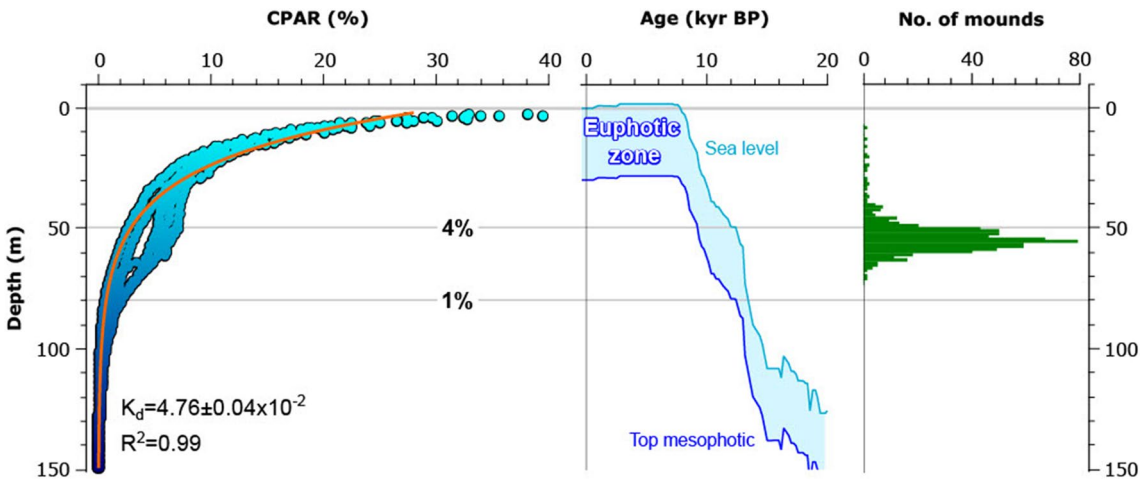

Fig. 11 Light and distribution of bioherms on the Tregrosse Bank. Left to right: Photosynthetic Available Radiation obtained during Expedition SO292 versus water depth since the last glacial cycle (Spratt and Lisiecki 2016) and infer depth of base of the euphotic zone (Lesser et al. 2009); depth distress of the top of the Halimeda bioherms on the bank (Fig. 1)

29 °C (Veron 2000). Similar conditions to those documented in the studied bioherms (Table 3). *Podabacia crustacea*, the other main species in the bioherms (Fig. 9E), has similar requirements as is the case for *Pachyseris speciosa,* and it is also typical of environments with restricted light conditions in depth between 20 and 40 m and water temperatures between 30 and 32 °C (Yusuf and Allen 2001) or 22–28 °C (Veron 2000). However, these corals in the present day at the Tregrosse Bank occur within waters with little light restriction (Table 3).

There are studies that suggest that the depth distribution of *Pachyseris speciosa* is not limited by light availability (Chow et al. 2019). The presence of *Pachyseris speciosa* in a wide range of depths indicates its capability to survive over a broad range of light regimes (Hernandez-Agreda et al. 2016). Chow et al. (2019) proposed temperature and the occurrence of downward flows of suspended particulate matter as the only significant parameters with negative effects on the development of *Pachyseris*. White et al. (2013) showed that platy corals, especially *Pachyseris*, are especially susceptible to breakage, even at a water depth exceeding 30 m. In the Great Barrier Reef, under storm conditions similar as the Queensland Plateau, Bongaerts (2022) reported extensive areas of plate-like coral rubble of *Pachyseris* and *Pobadacia* at depths between 50 and 65 m, which are directly comparable to the situation observed in the coral-debris belt of the studied bioherms of Tregrosse Bank (Fig. 8).

Development of the bioherms: sediment reworking and *Halimeda* growth

The coral-debris belt (Fig. 8) found around the reefs in the central part of the bioherms is the result of breakage of the corals and of sediment remobilization. Herbivory may be an important factor in the distribution of *Halimeda* (Castro-Sanguino et al. 2020). The low abundance of fish observed during the OFOS observations indicate, however, that fish activity is of limited significance, at least at the time of the study. Internal waves and bottom currents have been also suggested as important sediment transport mechanisms around mesophotic reefs (Pomar et al. 2012; Betzler et al. 2023; Bialik et al. 2023), but no evidence for them can be identified in the Tregrosse Bank. Finally, gravity-driven down-flank sediment transport is discarded as potential origin of the coral-debris belt since the slope of the flanks of the *Halimeda* bioherms, around 2°, is not steep enough to remobilize such coarse material.

By elimination, storm-wave-induced currents are proposed as the main mechanism for reef breakage and sediment mobilization. At shallow depths (< 100 m), wave-induced currents are important mechanisms for resuspending sediments (Butman et al. 1979; Fenton and Wilson 1985). Butman et al. (1979) found that wave- or tide-induced oscillatory flows are the most important process for resuspending the sediment in shallow platforms. Most recent studies analysing the effects of typhoons on mesophotic reefs reported that strong storms may destroy and (re)mobilize the reef framework (White et al. 2013; Bongaerts 2022; Turner et al. 2017). We propose an equivalent mechanism for the formation of the coral-debris belt in the studied *Halimeda* bioherms. The profound sediment reworking by these currents derived from storms may also be the cause of the homogenization of radiocarbon ages recorded in the upper centimetres of the *Halimeda* rudstone (Table 1).

In the Queensland Plateau, trade winds mainly blow towards the northwest, while surface currents flow from the east, mainly related to the North Caledonian Jet (Kessler and Cravatte 2013). This region is highly susceptible to tropical cyclones generated in the Pacific and preceding uninterrupted through the Queensland Plateau (Bloemendaal et al. 2020). Storms moving from east to west over the bioherms may damage the platy corals and redistributed the rubble with the slight windward–leeward asymmetry observed in some bioherms (Fig. 4). The asymmetry on the storm-remobilized material occurs on the surficial extension of the coralgal debris facies belt (Fig. 4A), poorly developed in the windward side of one of the bioherms, but also in its internal architecture (Fig. 4B). In any case, the corals debris form the substrate for subsequent *Halimeda* colonization.

Halimeda algae have a wide bathymetric range, from 0 to 150 mbsl, and can grow on a variety of substrates from unconsolidated mud to hard substrates (Jensen et al. 1985; Littler et al. 1988; Fong and Paul 2011, Williams et al. 2013). With some *Halimeda* species specifically adapted to deep-water/low-light habitats (Blair and Norris 1988; Littler et al. 1988). Given these low requirements and adaptations, it is difficult to determine the cause for the greater abundance of living *Halimeda* plants in topographic highs. The conventional view is that *Halimeda* mounds develop in nutrient-rich environments, as was reported in the Great Barrier Reef (Wolanski et al. 1988; Marshall and Davies 1988; Drew 2001; McNeil et al. 2016), Java Sea (Roberts et al. 1988), and the Caribbean Sea (Hine et al. 1988; Roberts et al. 1992; Teichberg et al. 2013). This was also extrapolated into the geological past (Mankiewicz 1988; Reolid et al. 2014). However, the relation between *Halimeda* and nutrients is not as straight forward. While *Halimeda*, like most algae, requires nutrients to flourish, the nutrient requirements of different species are very significant. *H.* tuna, for example, flourishes in the extremely nutrient-poor Eastern Mediterranean (Rilov et al. 2020; Ezra et al. 2021). High nutrient load may also hamper mineralization in some *Halimeda* species (Demes et al. 2009). As such, there are optimal nutrient domains, which likely differ between *Halimeda* species.

The western Coral Sea is relatively nutrient poor, even relative to the eastern Coral Sea (Dupouy et al. 2012),

with nutrients being depleted along their flow westwards. The low productivity also limits nutrient recycling due to remineralization of sinking organic matter. However, enough organic matter is being remineralization at depth to initiate a shallow nutricline, situated between 70 and 80 mbsl (Rissik et al. 1997; Ceccarelli et al. 2013) for both PO_4 and NO_x, although it is deeper for silica. Overall, the Coral Sea is considered N-limited at the surface (Browning and Moore 2023).

The bulk of the *Halimeda* mounds identified on the Tregrosse Bank appear to be situated just above the shallow nutricline, at depths of 40–70 mbspl (Fig. 2 and Table 2). The low chlorophyll values around the studied bioherms (Table 3) are consistent with low productivity of the surficial water above the nutricline at the time of the expedition. Thus, it appears that the studied bioherms represent a case of nutrient-poor *Halimeda* mounds. It does not necessarily mean that conditions are habitually nutrient poor in the study area. While upwelling is not reported around the Queensland Plateau, the main nutrient supply to the surface would be through a seasonal remixing following intense storms. Internal tides, identified at depths of 50–100 mbsl in the Coral Sea (Bendinger et al. 2023), may also result in pulsed input of nutrients. *Halimeda* may utilize opportunistic strategy, growing and multiplying rapidly in short pulses when nutrients are optimal (Smith et al. 2004). The development of *Halimeda* bioherms in the nutrient-poor waters of the Queensland Plateau (Ceccarelli et al. 2013), therefore, is unique amongst the rest of *Halimeda* buildups elsewhere.

With respect to the preferential occurrence of *Halimeda* plants on the mounds, in contrast with their scarcity in the flat areas of the Tregrosse Bank, McNeil et al. (2021a, b) proposed topographic elevation on the ring crests and the subsequent enhanced access to nutrients as the origin of the annulated *Halimeda* bioherms of the Great Barrier Reef. However, as already stated, the nutrients availability should be similar in the mounds and the flat areas of the Tregrosse Bank, both above the nutricline. Thus, nutrients are not the factor controlling the occurrence of the living *Halimeda* plant facies belt in the mounds.

Riding et al. (1991) proposed coral debris as the ideal substrate for *Halimeda* growth in fossil examples of the Miocene of South East Spain (Mankiewicz 1988; Braga and Martín 1996; Reolid et al. 2014; 2017). Perhaps, the availability of hard substrates, such as the coralgal debris facies belt (Table 4), is a key factor controlling the distribution and development of *Halimeda* bioherms, in addition to nutrient availability. However, a simpler and most possible advantage leading to living *Halimeda* on the bioherms, or to form them, but not living on the platform flat is for avoiding routinely be smothered by sediments being moved around (Figs. 3, 4, and 10).

Conclusions

This work presents morphology, internal structure, and in situ facies distribution of mesophotic *Halimeda* bioherms from the Queensland Plateau (NE Australia) and proposes the definition of a new bioherm morphotype. The characterization of this new type of *Halimeda* bioherms relies on hydroacoustic data, seafloor observations, oceanographic data, and discrete sediment sampling.

The studied *Halimeda* bioherms consist of cone-like buildups up to 500 m in diameter and between 3 and 10 m high with respect to the local baseline. They have gentle slopes between 2° and 5° and occur at water depths comprised between 10 and 70 mbsl, being especially abundant between 50 and 65 mbsl. Their internal structure consists of aggrading low-amplitude reflections at the core of the bioherm interfingering with high-amplitude reflections to the flanks. With respect to their surface facies distribution, the bioherms may be exclusively colonized by living *Halimeda* plants or present up to four facies belts, from distal to proximal: *Halimeda* rudstone, *Halimeda* rudstone with living plants, *Halimeda* rudstone with coralgal debris, and coralgal boundstone (when present, occupies the top of the bioherms). The *Halimeda* rudstone dominating the facies is recent but strongly reworked in its upper decimetres and has an average age of few decades.

We propose the alternation of two processes to explain the formation of the *Halimeda* bioherms on the Queensland Plateau: (1) accumulation of *Halimeda* debris and (2) episodic dismantling of the mesophotic coralgal boundstone at the centre of the bioherm. The mesophotic corals might be periodically affected by strong bottom currents caused by severe storms and cyclones that partially dismantle the reef and export coralgal rubble to the flanks. During fair-weather periods, *Halimeda* recolonize the flanks partially or completely covering the coralgal debris belt. This alternation of intervals dominated by coral debris with intervals dominated by *Halimeda* rudstone, may explain the interfingering between low-amplitude (coral rubble) and high-amplitude (*Halimeda* gravel) reflections imaged in the sub-bottom profiles. This processes likely started during the mid-last deglacial, around 14 kyr ago, since all the bioherms of the Tregrosse Bank have their bases on minor elevations of a distinct and continuous seismic reflector, likely produced during the subaerial exposure of the platform top following the sea-level fall to the LGM.

The development of *Halimeda* bioherms in the nutrient-poor waters of the Queensland Plateau, therefore, is unique amongst other *Halimeda* bioherms elsewhere. Due to their different depth of occurrence, geomorphology, complex internal structure, and surficial facies distribution, as well as their oligotrophic origin, we propose the buildups of the

Queensland Plateau represent a new *Halimeda* bioherm morphotype.

Acknowledgements The cruise SO292 was funded through grant 03G0292A—ICECARB from the Bundesministerium für Bildung und Forschung (Germany) to CB. We are grateful to captain Oliver Meyer, his officers and crew of RV SONNE for their excellent support. Many thanks to the technicians and the scientific party of cruise SO292. Thanks to L. Budke for OFOS data post-processing. JRs research was supported by the Spanish Ministry of Science and Innovation (MCIN) through the Ramón y Cajal Project RYC2021-034362-I (MCIN/AEI/https://doi.org/10.13039/501100011033 and NextGenerationEU/PRTR). We thank Parks Australia for the research permit for Cruise SO292 (permit EPBC 2022/9168), as well as Editor Morgan S. Pratchett and two anonymous reviewers for their valuable comments. The Schmidt Ocean Institute is thanked for the RV Falkor multibeam data acquired during cruises FK200429 and FK200802.

Funding Funding for open access publishing: Universidad de Granada/CBUA.

Declarations

Conflict of interest The authors declare no competing interests.

References

Beaman RJ (2020) High-resolution depth model for the Great Barrier Reef and Coral Sea - 100 m. Geoscience Australia, Canberra. https://doi.org/10.26186/5e2f8bb629d07

Bendinger A, Cravatte S, Gourdeau L, Brodeau L, Albert A, Tchilibou M, Lyard F, Vic C (2023) Regional modeling of internal-tide dynamics around New Caledonia-Part 1: Coherent internal-tide characteristics and sea surface height signature. Ocean Sci 19:1315–1338

Betzler C, Kroon D, Gartner S, Wei W (1993) Eocene to Miocene chronostratigraphy of the Queensland Plateau. Proc Ocean Drill Program, Sci Results 113:281–289

Betzler C, Eberli GP, Kroon D, Wright JD, Swart PK, Nath BN, Alvarez-Zarikian CA, Alonso-García M, Bialik OM, Blättler CL, Guo JA, Haffen S, Horozal S, Inoue M, Jovane L, Lanci L, Laya JC, Mee ALH, Lüdmann T, Nakakuni M, Niino K, Petruny LM, Pratiwi SD, Reijmer JJG, Reolid J, Slagle AL, Sloss CR, Su X, Yao Z, Young JR (2016) The abrupt onset of the modern South Asian Monsoon winds. Sci Rep 6:29838

Betzler C, Lindhorts S, Reijmer JJG, Braga JC, Lüdmann T, Bialik OM, Reolid J, Ge ßnner AL, Hainbucher D, Bisseur D, (2023) Carbonate platform drowning caught in the act: The sedimentology of Saya de Malha Bank (Indian Ocean). Sedimentology 70:78–99

Bialik OM, Gadol O, Micallef A, Betzler C, Nativ H, Einbinder S, Makovsky Y (2023) Internal waves and bottom currents interactions around mesophotic reefs, southeastern Mediterranean. eartharxiv.org

Blair SM, Norris JN (1988) The deep-water species of *Halimeda* Lamouroux (Halimedaceae, Chlorophyta) from San Salvador Island, Bahamas: species composition, distribution and depth records. Coral Reefs 6:227–236

Bloemendaal N, Haigh ID, de Moel H, Muis S, Haarsma RJ, Aerts JCJH (2020) Generation of a global synthetic tropical cyclone hazard dataset using STORM. Sci Data 7:40

Bongaerts P (2022) Mesophotic coral ecosystems. Curr Biol 32:R345–R346

Braga JC, Martín JM (1996) Geometries of reef advance in response to relative sea-level changes in a Messinian (uppermost Miocene) fringing reef (Cariatiz reef, Sorbas Basin, SE Spain). Sediment Geol 107:61–81

Browning TJ, Moore CM (2023) Global analysis of ocean phytoplankton nutrient limitation reveals high prevalence of co-limitation. Nat Commun 14:5014

Butman B, Noble M, Folger DW (1979) Long-term observations of bottom current and bottom sediment movement on the mid-Atlantic continental shelf. J Geophys Res Ocean 84:1187–1205

Castro-Sanguino C, Bozec Y, Mumby P (2020) Dynamics of carbonate sediment production by *Halimeda*: implications for reef carbonate budgets. Mar Ecol Prog Ser 639:91–106

Ceccarelli DM, McKinnon AD, Andréfouët S, Allain V, Young J, Gledhill DC, Flynn A, Bax NJ, Beaman R, Borsa P, Brinkman R, Bustamante RH, Campbell R, Cappo M, Cravatte S, D'Agata S, Dichmont CM, Dunstan PK, Dupouy C, Edgar G, Richardson AJ (2013) The Coral Sea: physical environment, ecosystem status and biodiversity assets. Advances Mar Biol 66(1):213–290. https://doi.org/10.1016/B978-0-12-408096-6.00004-3

Chow GSE, Chan YKS, Jain SS, Huang D (2019) Light limitation selects for depth generalists in urbanised reef coral communities. Mar Environ Res 147:101–112

Munsell Color (2021) Munsell soil-color charts: with genuine Munsell color chips. Munsell Color,

Cumings ER (1932) Reefs or Bioherms? Geol Soc Am Bull 43:331–352

Davies PJ (2011) *Halimeda* Bioherms. In: Hopley D (ed) Encyclopedia of Modern Coral Reefs Encyclopedia of Earth Sciences Series. Springer, Dordrecht, pp 539–549

Demes KW, Bell SS, Dawes CJ (2009) The effects of phosphate on the biomineralization of the green alga, Halimeda incrassata (Ellis) Lam. J of Experimental Mar Biol and Ecol 374:123–127

Drew EA (2001) Ocean nutrients to sediment banks via tidal jets and *Halimeda* meadows. In: Wolanski E (ed) Oceanographic processes of coral reefs: physical and biological links in the Great Barrier Reef. CRC Press LLC, Florida, pp 255–267

Drew EA, Abel KM (1988) Studies on *Halimeda*. Coral Reefs 6:195–205

Dunham RJ (1962) Classification of Carbonate Rocks According to Depositional Textures. In: Ham WE (ed) Classification of Carbonate Rocks, a Symposium. AAPG, Memoir

Dupouy C, Wattelez G, Fuchs R, Lefevre J, Mangeas M, Murakami H, Frouin R (2012) July. The colour of the Coral Sea. In 12th International Coral Reef Symposium (pp. ICRS2012–18E)

Embry AF, Klovan JE (1971) A Late Devonian reef tract on northeastern Banks Island, NWT. Bull Can Pet Geol 19:730–781

Ezra TB, Krom MD, Tsemel A, Berman-Frank I, Herut B, Lehahn Y, Rahav E, Reich T, Thingstad TF, Sher D (2021) Seasonal nutrient

dynamics in the P depleted eastern Mediterranean Sea. Deep Sea Research Part I: Ocean Res Papers 176:103607
Feary DA, Champion DC, Bultitude RJ, Davies PH (1993) Igneous and Metasedimentary Basement Lithofacies of the Queensland Plateau (Sites 824 and 825). Proc Ocean Drill Program, 133 Sci Results 133:535–540
Fenton MW, Wilson CJL (1985) Shallow-water turbidites: An example from the Mallacoota Beds, Australia. Sediment Geol 45:231–260
Fong P, Paul VJ (2011) Coral Reef Algae. In: Dubinsky Z, Stambler N (eds) Coral Reefs: An Ecosystem in Transition. Springer, Netherlands, Dordrecht, pp 241–272
Fournier F, Teillet T, Licht A, Borgomano J, Montaggioni L (2024) Eocene-Oligocene large-scale circulation of the East Asian summer monsoon recorded in neritic carbonates of the proto-South China Sea. Palaeogeogr Palaeoclimatol Palaeoecol 633:111883
Freile-Pelegrin Y, Robledo DR, García-Reina G (1995) Seasonal agar yield and quality inGelidium canariensis (Grunow) Seoane-Camba (Gelidiales, Rhodophyta) from Gran Canaria, Spain. J Appl Phycol 7:141–144
Ganachaud A, Cravatte S, Melet A, Schiller A, Holbrook NJ, Sloyan BM, Widlansky MJ, Bowen M, Verron J, Wiles P, Ridgway K, Sutton P, Sprintall J, Steinberg C, Brassington G, Cai W, Davis R, Gasparin F, Gourdeau L, Hasegawa T, Kessler W, Maes C, Takahashi K, Richards KJ, Send U (2014) The Southwest Pacific Ocean circulation and climate experiment (SPICE). J Geophys Res Ocean 119:7660–7686
Groeneveld J, Henderiks J, Renema W, McHugh CM, De Vleeschouwer D, Christensen BA, Fulthorpe CS, Reuning L, Gallagher SJ, Bogus K, Auer G, Ishiwa T (2017) Australian shelf sediments reveal shifts in Miocene Southern Hemisphere westerlies. Sci Adv 3:e1602567
Harney JN, Fletcher CH (2003) A Budget of Carbonate Framework and Sediment Production, Kailua Bay, Oahu. Hawaii J Sediment Res 73:856–868
Harney JN, Grossman EE, Richmond BM, Fletcher CH III (2000) Age and composition of carbonate shoreface sediments, Kailua Bay, Oahu. Hawaii Coral Reefs 19:141–154
Heaton TJ, Köhler P, Butzin M, Bard E, Reimer RW, Austin WEN, Bronk Ramsey C, Grootes PM, Hughen KA, Kromer B, Reimer PJ, Adkins J, Burke A, Cook MS, Olsen J, Skinner LC (2020) Marine20—The Marine Radiocarbon Age Calibration Curve (0–55,000 cal BP). Radiocarbon 62:779–820
Hernandez-Agreda A, Leggat W, Bongaerts P, Ainsworth TD (2016) The microbial signature provides insight into the mechanistic basis of coral success across reef habitats. MBio 7(4):1–10. https://doi.org/10.1128/mBio.00560-16
Hine AC, Hallock P, Harris MW, Mullins HT, Belknap DF, Jaap WC (1988) *Halimeda* bioherms along an open seaway: Miskito Channel, Nicaraguan Rise, SW Caribbean Sea. Coral Reefs 6:173–178
Hughes TP (1989) Community Structure and Diversity of Coral Reefs: The Role of History. Ecology 70:275–279
Iwase A, Sakai K, Suzuki A, van Woesik R (2008) Phototropic adjustment of the foliaceous coral Echinopora lamellosa in Palau. Estuar Coast Shelf Sci 77(4):672–678
Jensen PR, Gibson RA, Littler MM, Littler DS (1985) Photosynthesis and calcification in four deep-water *Halimeda* species (chlorophyceae, caulerpales). Deep Sea Res Part A Oceanogr Res Pap 32:451–464
Kessler WS, Cravatte S (2013) Mean circulation of the Coral Sea. J Geophys Res Ocean 118:6385–6410
Lesser MP, Slattery M, Leichter JJ (2009) Ecology of mesophotic coral reefs. J Exp Mar Bio Ecol 375:1–8
Lewis SE, Sloss CR, Murray-Wallace CV, Woodroffe CD, Smithers SG (2013) Post-glacial sea-level changes around the Australian margin: a review. Quat Sci Rev 74:115–138
Littler MM, Littler DS, Lapointe BE (1988) A comparison of nutrient- and light-limited photosynthesis in psammophytic versus epilithic forms of *Halimeda* (Caulerpales, Halimedaceae) from the Bahamas. Coral Reefs 6:219–225
Mankiewicz C (1988) Occurrence and paleocologic significance of *Halimeda* in late Miocene reefs, southeastern Spain. Coral Reefs 6:271–279
Marshall JF, Davies P (1988) *Halimeda* bioherms of the northern Great Barrier Reef. Coral Reefs 6:139–148
Martín JM, Braga J, Riding R (1997) Late Miocene *Halimeda* algal-microbial segment reefs in the marginal Mediterranean Sorbas Basin, Spain. Sedimentology 44:441–456
McNeil MA, Webster JM, Beaman RJ, Graham TL (2016) New constraints on the spatial distribution and morphology of the *Halimeda* bioherms of the Great Barrier Reef, Australia. Coral Reefs 35:1343–1355
McNeil MA, Firn J, Nothdurft LD, Pearse AR, Webster JM, Roland Pitcher C (2021a) Inter-reef *Halimeda* algal habitats within the Great Barrier Reef support a distinct biotic community and high biodiversity. Nat Ecol Evol 5:647–655
McNeil MA, Nothdurft LD, Dyriw NJ, Webster JM, Beaman RJ (2021b) Morphotype differentiation in the Great Barrier Reef *Halimeda* bioherm carbonate factory: Internal architecture and surface geomorphometrics. Depos Rec 7:176–199
McNeil MA, Nothdurft LD, Hua Q, Webster JM, Moss P (2022) Evolution of the inter-reef *Halimeda* carbonate factory in response to Holocene sea-level and environmental change in the Great Barrier Reef. Quat Sci Rev 277:107347
Mollenhauer G, Grotheer H, Gentz T, Bonk E, Hefter J (2021) Standard operation procedures and performance of the MICADAS radiocarbon laboratory at Alfred Wegener Institute (AWI), Germany. Nucl Instruments Methods Phys Res Sect B Beam Interact with Mater Atoms 496:45–51
Müller RD, Lim VS, Isern AR (2000) Late Tertiary tectonic subsidence on the northeast Australian passive margin: response to dynamic topography? Mar Geol 162:337–352
Mutter JC (1977) The Queensland Plateau. Bureau of Mineral Resources, Geology and Geophysics, Bulletin 179,
Orme GR, Salama MS (1988) Form and seismic stratigraphy of *Halimeda* banks in part of the northern Great Barrier Reef Province. Coral Reefs 6:131–137
Orme GR, Flood PG, Sargent GEG (1978) Sedimentation trends in the lee of outer (ribbon) reefs, Northern Region of the Great Barrier Reef Province. Philos Trans R Soc London Ser a, Math Phys Sci 291:85–99
Phipps CVG, Roberts HH (1988) Seismic characteristics and accretion history of *Halimeda* bioherms on Kalukalukuang Bank, eastern Java Sea (Indonesia). Coral Reefs 6:149–159
Pomar L, Morsilli M, Hallock P, Bádenas B (2012) Internal waves, an under-explored source of turbulence events in the sedimentary record. Earth Sci Rev 111:56–81
Rees SA, Opdyke BN, Wilson PA, Henstock TJ (2007) Significance of *Halimeda* bioherms to the global carbonate budget based on a geological sediment budget for the Northern Great Barrier Reef, Australia. Coral Reefs 26:177–188
Reimer PJ, Brown TA, Reimer RW (2004) Discussion: Reporting and Calibration of Post-Bomb 14 C Data. Radiocarbon 46:1299–1304
Reimer R, Reimer P (2004) CALIBomb-calibration of post-bomb C-14 data.
Reolid J, Betzler C, Braga JC, Martín JM, Lindhorst S, Reijmer JJG (2014) Reef slope geometries and facies distribution: controlling factors (Messinian, SE Spain). Facies 60:737–753
Reolid J, Betzler C, Singler V, Stange C, Lindhorst S (2017) Facies variability in mixed carbonate–siliciclastic platform slopes (Miocene). Facies 63:11

Riding R, Martín JM, Braga JC (1991) Coral-stromatolite reef framework, Upper Miocene, Almeria, Spain. Sedimentology 38:799–818

Rilov G, Peleg O, Guy-Haim T, Yeruham E (2020) Community dynamics and ecological shifts on Mediterranean vermetid reefs. Mar Env Res 160:105045

Rissik D, Suthers IM, Taggart CT (1997) Enhanced zooplankton abundance in the lee of an isolated reef in the south Coral Sea: the role of flow disturbance. J of Plankton Res 19:1347–1368

Robbins LL, Knorr PO, Hallock P (2009) Response of *Halimeda* to ocean acidification: field and laboratory evidence. Biogeosciences Discuss 6:4895–4918

Roberts HH, Aharon P, Phipps CV (1988) Morphology and sedimentology of Halimeda bioherms from the eastern Java Sea (Indonesia). Coral Reefs 6:161–172

Roberts HH, Wilson PA, Lugo-Fernández A (1992) Biologic and geologic responses to physical processes: examples from modern reef systems of the Caribbean-Atlantic region. Cont Shelf Res 12:809–834

Sinutok S, Hill R, Doblin MA, Kühl M, Ralph PJ (2012) Microenvironmental changes support evidence of photosynthesis and calcification inhibition in *Halimeda* under ocean acidification and warming. Coral Reefs 31:1201–1213

Smith JE, Smith CM, Vroom PS, Beach KL, Miller S (2004) Nutrient and growth dynamics of *Halimeda* tuna on Conch Reef, Florida Keys: Possible influence of internal tides on nutrient status and physiology. Limnol Oceanogr 49:1923–1936

Spalding HL (2012) Ecology of mesophotic macroalgae and *Halimeda* kanaloana meadows in the Main Hawaiian Islands. University of Hawaii at Manoa

Spratt RM, Lisiecki LE (2016) A Late Pleistocene sea level stack. Clim past 12:1079–1092

Stuiver M, Reimer PJ (1993) Extended 14 C Data Base and Revised CALIB 3.0 14 C Age Calibration Program. Radiocarbon 35:215–230

Tanner JE (1995) Competition between scleractinian corals and macroalgae: An experimental investigation of coral growth, survival and reproduction. J Exp Mar Bio Ecol 190:151–168

Teichberg M, Fricke A, Bischof K (2013) Increased physiological performance of the calcifying green macroalga *Halimeda* opuntia in response to experimental nutrient enrichment on a Caribbean coral reef. Aquat Bot 104:25–33

Turak E, DeVantier L (2019) Bridge T.C.L. (eds) Reef-Building Corals of the Upper Mesophotic Zone of the Central Indo-West Pacific. In: Loya Y., Puglise K.A., Springer Cham

Turner JA, Babcock RC, Hovey R, Kendrick GA (2017) Deep thinking: a systematic review of mesophotic coral ecosystems. ICES J Mar Sci 74:2309–2320

Veron JEN (2000) Corals of the world. Australian Institute of Marine Science and CRR Qld.

White KN, Ohara T, Fujii T, Kawamura I, Mizuyama M, Montenegro J, Shikiba H, Naruse T, McClelland T, Denis V, Reimer JD (2013) Typhoon damage on a shallow mesophotic reef in Okinawa. Japan Peerj 1:e151

Wienberg C, Westphal H, Kwoll E, Hebbeln D (2010) An isolated carbonate knoll in the Timor Sea (Sahul Shelf, NW Australia): facies zonation and sediment composition. Facies 56:179–193

Williams GJ, Smith JE, Conklin EJ, Gove JM, Sala E, Sandin SA (2013) Benthic communities at two remote Pacific coral reefs: effects of reef habitat, depth, and wave energy gradients on spatial patterns. PeerJ 1:e81

Wolanski E, Drew E, Abel KM, O'Brien J (1988) Tidal jets, nutrient upwelling and their influence on the productivity of the alga *Halimeda* in the Ribbon Reefs, Great Barrier Reef. Estuar Coast Shelf Sci 26:169–201

Wu Y, Fallon SJ, Cantin NE, Lough JM (2021) Surface ocean radiocarbon from a porites coral record in the Great Barrier Reef: 1945–2017. Radiocarbon 63:1193–1203

Yokoyama Y, Esat TM, Thompson WG, Thomas AL, Webster JM, Miyairi Y, Sawada C, Aze T, Matsuzaki H, Okuno JI, Fallon S, Braga JC, Humblet M, Iryu Y, Potts DC, Fujita K, Suzuki A, Kan H (2018) Rapid glaciation and a two-step sea level plunge into the Last Glacial Maximum. Nature 559:603–607

Yusuf S, Allen G (2001) Conditions of coral reefs in the Togean and Banggai Islands, Sulawesi. Indonesia. In: Allen G., Werner T., McKenna S. (eds) A marine rapid assessment of the Togean and Banggai Islands, Sulawesi, Indonesia. RAP Bulletin of Biology Assessment 20, pp 27-37